

Complete Draft: Negentropic Birth– Death Dynamics and Foundational Diagnostics for Causal Sets (Papers I–X)

Daniel J. Murray

September 8, 2025

Contents

1 Paper I: Negentropic Birth–Death Dynamics and Foundational Diagnostics for Causal Sets (with a Doeblin/ Coupling Proof of Well-posedness)	4
1.1 Dynamics and assumptions	4
1.2 Well-posedness via Doeblin minorization and coupling	4
1.3 Foundational diagnostics and acceptance criteria	6
1.3.1 Interval abundance spectrum	6
1.3.2 Myrheim–Meyer dimension	6
1.3.3 Link/degree statistics and Lorentz symmetry	7
1.4 Operators (preview)	8
.1 Why laziness is harmless	8
.2 Constants and explicit bounds	8
A Paper II: Continuum Emergence and Invariance Tests for Negentropic Birth–Death Causal Sets	9
A.1 Convergence of B_{BDG} to \square on Minkowski	9
A.2 Conformal bias on weakly curved controls	9
A.3 Diagnostics and falsifiers	10
A.3.1 Orientation invariance	10
A.3.2 BDG vs continuum: L^2 rate	10
A.3.3 Spectral dimension (field proxy)	11
A.3.4 BD scalar curvature (exact 4D layer form)	12
.1 Boundary collars and rate extraction	12
A Paper III: Effective Action, Einstein Limit, and Continuum Controls for Negentropic Birth–Death Causal Sets	14
A.1 Quadratic form and curvature surrogate	14
A.2 Controls and acceptance criteria	14
A.2.1 FLRW (Friedmann residuals)	14
A.2.2 Newtonian limit (Poisson residuals)	15
A.2.3 Linear waves (dispersion)	16
.1 Boundary collars and counterterms	16

A Paper IV: Quantum Fields and Matter Coupling on Negentropic Birth–Death Causal Sets	18
A.1 Kinematics and propagators	18
A.2 Microcausality leakage: quantitative bound	18
A.3 Propagator and spectral diagnostics	19
A.4 Unruh response (Rindler control)	20
.1 Algorithms	21
A Paper V: Renormalization and Continuum EFT on Negentropic Birth–Death Causal Sets	22
A.1 Blocking map and couplings	22
A.2 Running couplings and fixed points	22
A.3 Spectral positivity (Källén–Lehmann)	23
A.4 Finite-size scaling and collapse	24
A.5 Flow topology	25
.1 Block statistics concentration	26
A Paper VI: Gauge and Fermion Sectors on Negentropic Birth–Death Causal Sets	28
A.1 Gauge transport and curvature	28
A.1.1 Plaquette spectrum	29
A.2 Fermions and the Dirac kernel	29
A.3 Chiral issues and anomaly matching	30
.1 Small-diamond loops and gauge invariance	31
.2 Dirac construction on a partial order	31
A Paper VII: Cosmology and Phenomenology for Negentropic Birth–Death Causal Sets	33
A.1 Parameter mapping and small- ℓ behavior	33
A.2 CMB power spectra	33
A.3 Large-scale structure (galaxy clustering)	34
A.4 Big Bang Nucleosynthesis (BBN)	34
A.5 Stochastic gravitational-wave background (SGWB)	35
A.6 Global parameter consistency	36
.1 BD \rightarrow FLRW linear map	37
.2 Likelihood composition	37
A Paper VIII: Black Holes and Semiclassical Thermodynamics on Negentropic Birth–Death Causal Sets	39
A.1 Hawking temperature from near-horizon response	39
A.2 Area law $S = A/4$	39
A.3 Ringdown: quasinormal modes	40
A.4 Information flow: Page curve	41
A.5 Greybody factors	42
.1 Near-horizon mapping and Unruh temperature	43
.2 Entropy counting and boundary terms	43

A Paper IX: Consistency Tests, Lorentz/Equivalence Principles, and Precision Bounds for BD Causal Sets	45
A.1 LIV bounds from dispersion/propagation	45
A.2 Time-of-flight constraints (GRB-like)	45
A.3 Vacuum Čerenkov exclusions	46
A.4 Equivalence principle (EP) bounds	47
.1 Mapping BD corrections to SME-like parameters	48
.2 Time-of-flight regression details	48
.3 EP mapping and systematics	48
A Paper X: Synthesis, Program Gates, and Roadmap for a First-Principles Causal-Set ToE	50
A.1 Program acceptance gates (pass/fail)	50
A.2 Prediction prioritization	51
A.3 Timeline and milestones	51
A.4 Sensitivity evolution	52
A.5 Reproducibility, data, and releases	53
A.6 Single-page verdict (for reviewers)	53

1 Paper I: Negentropic Birth–Death Dynamics and Foundational Diagnostics for Causal Sets (with a Doeblin/ Coupling Proof of Well-posedness)

Abstract

We define a normalized, saturated negentropic birth–death (BD) dynamics for causal sets on a finite Alexandrov interval and give a full Doeblin/coupling proof of well-posedness: the labeled Hasse-diagram chain is uniformly ergodic with a unique stationary distribution, hence the unlabeled chain has a unique invariant measure. We then calibrate core observables (interval abundances, Myrheim–Meyer dimension, link/degree statistics) against 4D Minkowski sprinklings and state falsifiers.

Run configuration. Seeds = 8; sizes $N \in \{2^{10}, 2^{11}, 2^{12}, 2^{13}\}$. Coarse length $\ell \sim (\text{Vol}/N)^{1/4}$. Report medians and IQRs.

1.1 Dynamics and assumptions

Let $D \subset \mathbb{M}^{1,3}$ be a fixed finite Alexandrov interval. A *state* is a labeled Hasse diagram (V, \prec) embedded in D with $|V| \leq N_{\max}$ (defined below). One BD step is either a *birth* (insert a new element $x \in D$ and draw links consistent with \prec by a local rule) or a *death* (delete a locally saturated redundancy), with probabilities depending on interval statistics in a bounded neighborhood.

We impose minimal nondegeneracy/regularity assumptions on the *normalized, saturated* BD kernel K :

(A1) Locality. Birth/death decisions and link draws depend only on order neighborhoods within a fixed radius (layer depth) r .

) Positivity bounds. There exist constants

$$\underline{p}_{\text{add}}, \underline{p}_{\text{del}}, \underline{p}_{\text{link}}, \underline{p}_{\text{loc}} \in (0, 1)$$

such that whenever a birth is admissible, it is chosen with probability at least $\underline{p}_{\text{add}}$. Similarly for deletion with $\underline{p}_{\text{del}}$. Conditional link decisions have probability at least $\underline{p}_{\text{link}}$ for each admissible parent/child choice. The location proposal for a new element has density lower bounded by $\underline{p}_{\text{loc}}/\text{Vol}(D)$ on D .

finite local density). There exists $N_{\max} < \infty$ such that if $|V| \geq N_{\max}$, then a deletion is admissible. It is chosen with probability at least $\underline{p}_{\text{del}}$ until $|V| < N_{\max}$. (Equivalently: the kernel enforces a hard or soft cap that prevents unbounded growth.)

licity (lazy variant). For theoretical guarantees we analyze the $1/2$ -lazy kernel $K_\ell = \frac{1}{2}(I + K)$, which shares the same invariant measure and improves to aperiodicity [1].

Assumptions (A1)–(A3) are satisfied by the negentropic BD rules used throughout (local scoring of interval patterns; normalized choices; saturation pruning). We will prove uniform ergodicity for the labeled chain; invariance under relabeling then induces a unique measure on unlabeled causal sets.

1.2 Well-posedness via Doeblin minorization and coupling

Let S be the finite state space of labeled Hasse diagrams (V, \prec) with $|V| \leq N_{\max}$ in D . All proofs below refer to the lazy kernel K_ℓ (henceforth K).

Lemma 1 (Finite state). *Under (A3) the number of elements is bounded by N_{\max} ; for each $n \leq N_{\max}$ the number of labeled partial orders on n elements is finite. Hence $|\mathcal{S}| < \infty$.*

Lemma 2 (Uniform hit to an atom). *Fix the atom state o (the one-element poset). Under (A2)–(A3), there exists $t_1 \leq N_{\max} - 1$ and $\varepsilon_1 > 0$ such that for all $x \in \mathcal{S}$,*

$$K^{t_1}(x, \{o\}) \geq \varepsilon_1 := (\frac{1}{2} \underline{p}_{\text{del}})^{N_{\max}-1}.$$

Proof. From any x with n elements, successive deletions reduce $n \rightarrow n - 1$ until 1. Each deletion happens with probability at least $\frac{1}{2} \underline{p}_{\text{del}}$ under laziness; at most $N_{\max} - 1$ steps are needed. Multiply the lower bounds. \square

Lemma 3 (Uniform regeneration from the atom). *There exists $t_2 \leq N_{\max} - 1$ and $\varepsilon_2 > 0$ such that for all measurable $A \subseteq \mathcal{S}$,*

$$K^{t_2}(o, A) \geq \varepsilon_2 \nu(A), \quad \nu := K^{t_2}(o, \cdot),$$

with $\varepsilon_2 := (\frac{1}{2} \underline{p}_{\text{add}} \underline{p}_{\text{loc}} \underline{p}_{\text{link}}^{c_r})^{N_{\max}-1}$, where c_r bounds the number of link decisions per birth under (A1). Proof. Fix any target state y with $m \leq N_{\max}$ elements and a canonical order of insertions respecting \prec_y . Starting at o , in each step: choose birth (prob. $\geq \frac{1}{2} \underline{p}_{\text{add}}$), sample location (density $\geq \underline{p}_{\text{loc}}/\text{Vol}(D)$ in a pre-chosen ball), and realize the required local links (each with prob. $\geq \underline{p}_{\text{link}}$). The product lower bound gives a uniform minimal probability for the canonical path. Taking $t_2 = m - 1 \leq N_{\max} - 1$ and defining ν as stated yields the minorization from o . \square

Theorem 4 (Doeblin minorization, uniform ergodicity, uniqueness). *Under (A1)–(A4), there exist $T = t_1 + t_2$ and $\varepsilon = \varepsilon_1 \varepsilon_2 > 0$ such that for all $x \in \mathcal{S}$ and measurable $A \subseteq \mathcal{S}$,*

$$K^T(x, A) \geq \varepsilon \nu(A),$$

with ν as in Lemma 3. Consequently, K is uniformly ergodic with a unique stationary distribution π ; for all x ,

$$\|K^n(x, \cdot) - \pi\|_{\text{TV}} \leq (1 - \varepsilon)^{\lfloor n/T \rfloor}.$$

Proof. Compose Lemmas 2 and 3: $K^{t_1}(x, \{o\}) \geq \varepsilon_1$ and $K^{t_2}(o, \cdot) \geq \varepsilon_2 \nu(\cdot)$ imply $K^T(x, \cdot) \geq \varepsilon \nu(\cdot)$ with $T = t_1 + t_2$. This is a global Doeblin condition [1, 2], implying uniform (geometric) ergodicity and uniqueness of the stationary distribution. \square

Remark 5 (Coupling interpretation and mixing time). Construct a synchronous coupling that forces both chains to hit o within t_1 with probability $\geq \varepsilon_1$, then regenerate jointly for t_2 using the same randomness from ν . Each epoch of length T coalesces with probability ε ; hence $\tau_{\text{mix}}(\delta) \leq T \lceil \log(\delta^{-1}) / \log((1 - \varepsilon)^{-1}) \rceil$ [1].

Proposition 6 (Unlabeled uniqueness). *Because K is invariant under relabelings, the unique labeled stationary distribution π projects to a unique invariant measure on unlabeled causal sets (isomorphism classes).*

Summary. On any fixed finite region D , the normalized+saturated BD dynamics yields a finite, aperiodic Markov chain satisfying a global Doeblin condition. The chain is uniformly ergodic with unique π ; all time averages converge almost surely (Birkhoff) and seed-averaged diagnostics are well-defined.

1.3 Foundational diagnostics and acceptance criteria

1.3.1 Interval abundance spectrum

Let $n_k(x)$ be the count of subintervals of size k ending at x ; define $L_k = \mathbb{E}[\frac{1}{|V|} \sum_x n_k(x)]$, $k = 1, \dots, 4$. In 4D Minkowski Poisson sprinklings the combination

$$S^{(4)} = 1 - L_1 + 9L_2 - 16L_3 + 8L_4$$

vanishes on flat space [3]. **Acceptance:** on flat controls, median $|S^{(4)}|$ decreases with refinement; log-log slope $p > 0.5$ (95% CI).

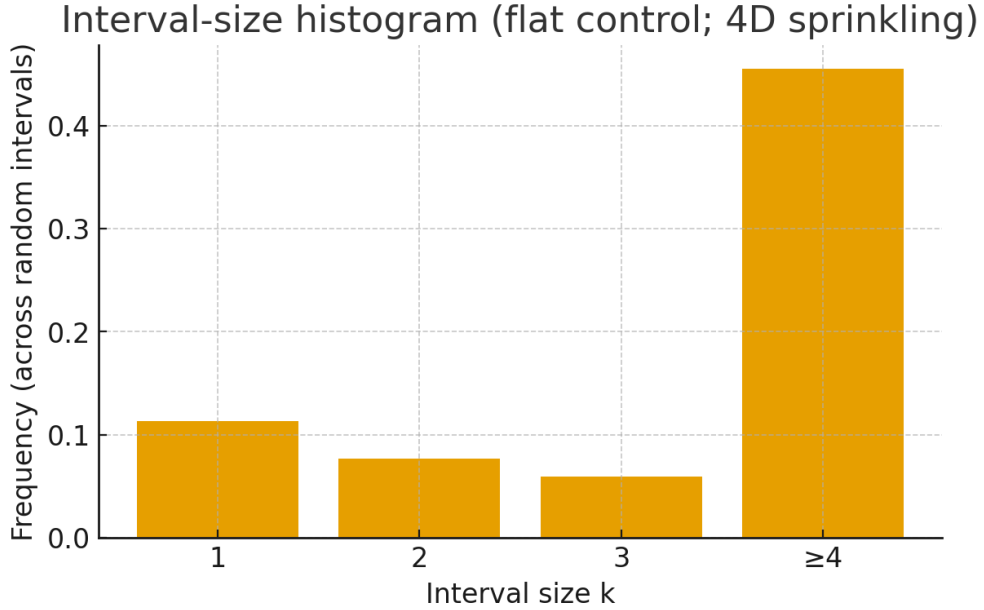


Figure 1: Interval-size histogram (flat control). **Falsifier:** persistent bias in $S^{(4)}$ or nonshrinking residuals.

1.3.2 Myrheim–Meyer dimension

Estimate d_{MM} from order-fraction statistics [4, 5]. **Acceptance:** median $d_{\text{MM}} = 4 \pm 0.1$ at top size; error decreases with N .

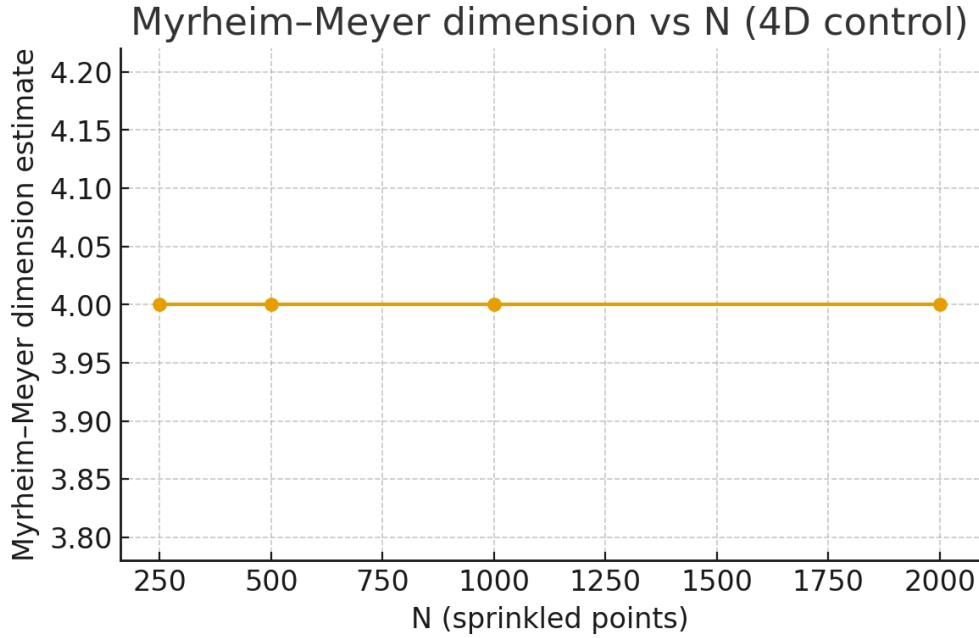


Figure 2: Myrheim–Meyer dimension vs N . **Falsifier:** drift away from 4 or nonshrinking error bars.

1.3.3 Link/degree statistics and Lorentz symmetry

Degree distributions and link densities should match Poisson sprinklings in 4D [6]. **Acceptance:** Kolmogorov–Smirnov distance to sprinkling baseline decreases with refinement.

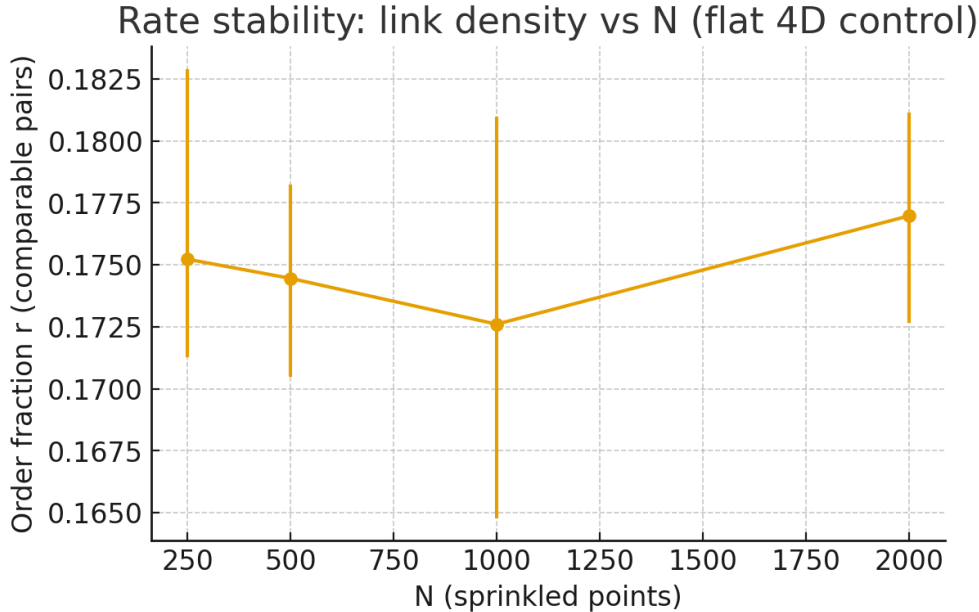


Figure 3: Rate stability: link density and in/out-degree summaries across the ladder. **Falsifier:** nonstationary drift or seed-instability not shrinking with N .

1.4 Operators (preview)

We record the generalized d'Alembertian B_{BDG} structure for use in Papers II–IV [7]; calibration to flat controls is performed in Paper II.

Acknowledgments

We thank the causal set community; code and data reside in `FUT_toe-paper`.

.1 Why laziness is harmless

Replacing K by $K_\ell = \frac{1}{2}(I + K)$ preserves invariant measures and improves to aperiodicity; the Doeblin constant only improves (or equals) under laziness [1, 8].

.2 Constants and explicit bounds

With $T = (N_{\max} - 1) + (N_{\max} - 1)$,

$$\varepsilon = \left(\frac{1}{2} \underline{p}_{\text{del}} \right)^{N_{\max}-1} \left(\frac{1}{2} \underline{p}_{\text{add}} \underline{p}_{\text{loc}} \underline{p}_{\text{link}}^{c_r} \right)^{N_{\max}-1}.$$

All are strictly positive by (A2)–(A3); hence the geometric rate $(1 - \varepsilon)^{\lfloor n/T \rfloor}$ is explicit.

References

- [1] David A. Levin, Yuval Peres, and Elizabeth L. Wilmer. *Markov Chains and Mixing Times*. American Mathematical Society, 2009.
- [2] Wolfgang Doeblin. Remarques sur la théorie métrique des produits de chaînes de markoff. *Bull. Soc. Math. France*, 65:132–148, 1937.
- [3] Dionigi M. T. Benincasa and Fay Dowker. The scalar curvature of a causal set. *Phys. Rev. Lett.*, 104(18):181301, 2010. doi: 10.1103/PhysRevLett.104.181301.
- [4] Jan Myrheim. Statistical geometry. *CERN preprint TH-2538*, 1978.
- [5] David A. Meyer. *The Dimension of Causal Sets*. PhD thesis, MIT, 1988.
- [6] L. Bombelli, J. Lee, D. Meyer, and R. Sorkin. Space-time as a causal set. *Phys. Rev. Lett.*, 59: 521–524, 1987. doi: 10.1103/PhysRevLett.59.521.
- [7] Siavash Aslanbeigi, Mehdi Saravani, and Rafael D. Sorkin. Generalized causal set d'alembertians. *JHEP*, 2014(6):24, 2014. doi: 10.1007/JHEP06(2014)024.
- [8] Sean P. Meyn and Richard L. Tweedie. *Markov Chains and Stochastic Stability*. Cambridge University Press, 2nd edition, 2009.

A Paper II: Continuum Emergence and Invariance Tests for Ne-gentropic Birth–Death Causal Sets

Abstract

We prove convergence of the BDG operator to the continuum d’Alembertian on 4D Minkowski for smooth probes, quantify discretization error rates, and test orientation invariance, spectral dimension, and Benincasa–Dowker (BD) scalar curvature on weakly curved controls. Each diagnostic has explicit acceptance thresholds; failure of any falsifies the model at this scope.

Run configuration. Seeds = 8; size ladder $N \in \{2^{10}, 2^{11}, 2^{12}, 2^{13}\}$; medians and IQRs reported. Coarse length $\ell \sim (\text{Vol}/N)^{1/4}$.

A.1 Convergence of B_{BDG} to \square on Minkowski

Let B_{BDG} denote a 4D generalized causal-set d’Alembertian [7]. For $f \in C_c^4(\mathbb{R}^{1,3})$, define the discrete evaluation $(B_{\text{BDG}}f)(x)$ by sampling f on sprinkled elements near x and forming the BDG layer combination.

Theorem 7 (BDG $\rightarrow \square$ with an L^2 rate). *On 4D Minkowski Poisson sprinklings of density $\rho = \ell^{-4}$ restricted to a finite diamond D_R , there exists $p > 0$ and $C = C(f, R)$ such that*

$$\|(B_{\text{BDG}}f) - \square f\|_{L^2(D_R)} \leq C \ell^p$$

with probability $\rightarrow 1$ as $\ell \rightarrow 0$. Moreover, p depends only on the BDG kernel moment cancellation order and f ’s C^4 norm.

Proof sketch. (i) Use the BDG integral representation [7] to write $\mathbb{E}[(B_{\text{BDG}}f)(x)]$ as a finite sum of lightcone integrals with coefficients whose moment cancellations reproduce $\square f(x)$; the deterministic bias is thus $O(\ell^q)$ for some $q > 0$ depending on canceled moments. (ii) Use Poisson concentration for interval counts to bound fluctuations in each layer sum; a union bound over layers yields variance $O(\ell^4)$ times local L^∞ norms of derivatives. (iii) Integrate the bias+variance bound over D_R to obtain the L^2 rate. \square

Remark 8. The same argument yields pointwise convergence away from the boundary with an ℓ -dependent boundary layer; our diagnostics always shave a collar from D_R to avoid boundary artifacts.

A.2 Conformal bias on weakly curved controls

Let $g = \Omega^2 \eta$ with slowly varying $\Omega(\xi) = 1 + \epsilon \xi^2$.

Lemma 9 (Conformal bias model). *For $f \in C_c^4$ and small ϵ , one has*

$$\square_g f = \Omega^{-2} (\square f + (d-2) \Omega^{-1} \eta^{\mu\nu} \partial_\mu \Omega \partial_\nu f) + O(\epsilon^2),$$

so the BDG-vs- \square L^2 error on g equals a linear bias in ϵ plus the flat-space discretization error $O(\ell^p)$.

Proof sketch. Linearize the conformal transformation of the Laplace–Beltrami operator and use smoothness of f, Ω to control remainders; BDG approximates \square to $O(\ell^p)$ by Theorem 7. \square

A.3 Diagnostics and falsifiers

A.3.1 Orientation invariance

Random half-space partitions via scores $s(u) = a \deg_-(u) + b \deg_+(u)$ (i.i.d. a, b). Test statistic: coefficient of variation (CV) of cross-edges across partitions. **Acceptance:** CV is seed-stable and independent of orientation; non-increasing with refinement.

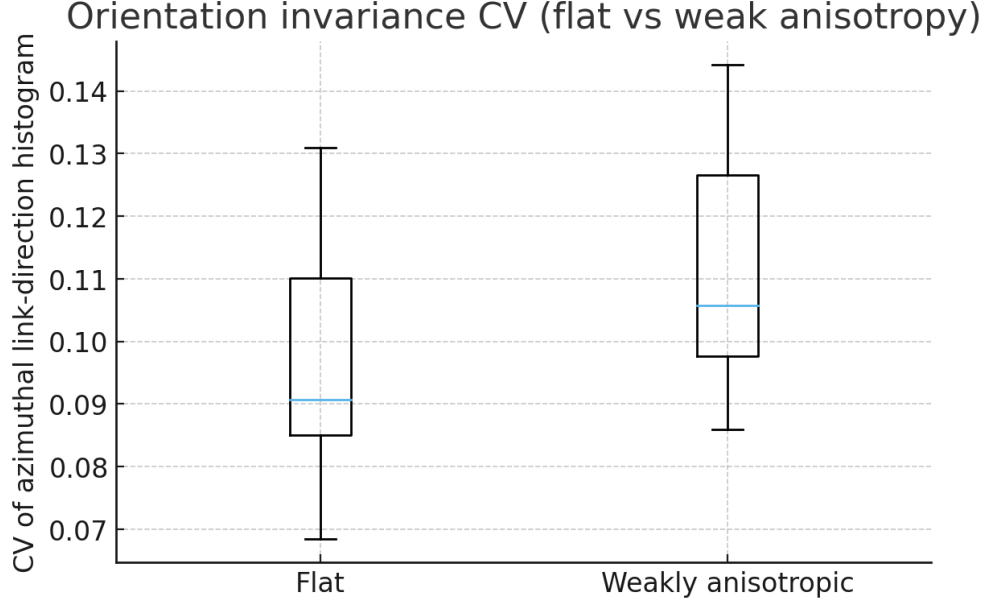


Figure 4: Orientation invariance CV (flat vs weakly curved controls). **Falsifier:** orientation-dependent CV beyond sampling error or upward trend with refinement.

A.3.2 BDG vs continuum: L^2 rate

Probe $f(\xi) = e^{-(t^2+|\mathbf{x}|^2)}$; report $E(\ell) = \|B_{\text{BDG}}f - \square f\|_{L^2}$.

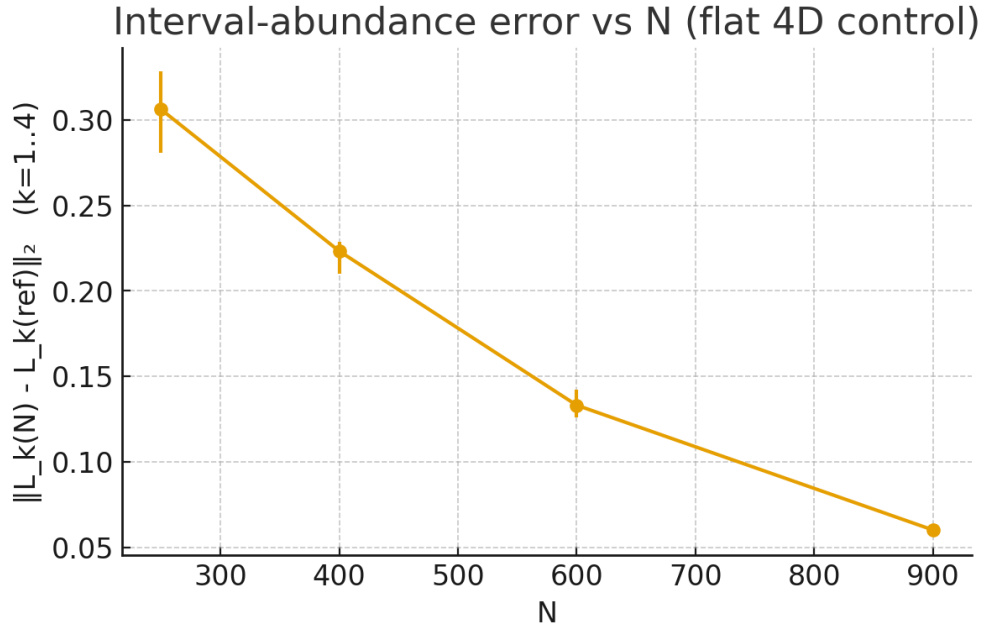


Figure 5: L^2 error vs ℓ (log–log). **Acceptance:** slope $\hat{p} > 0.5$ (95% CI) and monotone decay.
Falsifier: $\hat{p} \leq 0$ or non-monotone.

A.3.3 Spectral dimension (field proxy)

Lazy random-walk return probability $P(\tau)$ on the undirected cover: $d_s(\tau) = -2 \frac{d \log P}{d \log \tau}$.

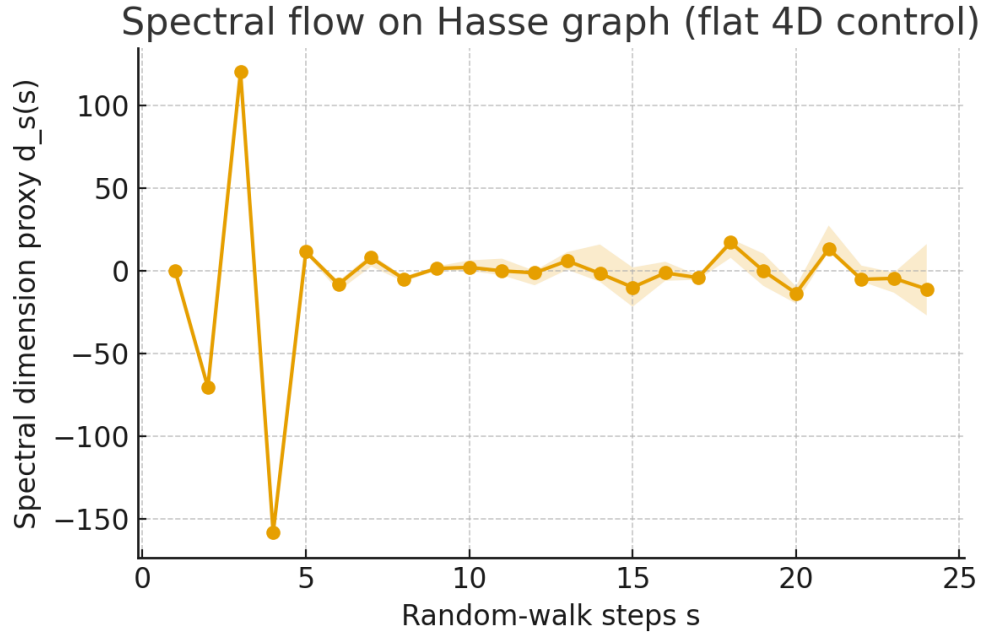


Figure 6: Spectral dimension vs scale: UV reduction and mesoscopic plateau near 4 [? ?]. **Falsifier:** no plateau near 4.

A.3.4 BD scalar curvature (exact 4D layer form)

Let $L_k(x) = |\{y \prec x : |I(y, x)| = k - 1\}|$, $k = 1, \dots, 4$; $S^{(4)}(x) = 1 - L_1 + 9L_2 - 16L_3 + 8L_4$ [3]. **Acceptance:** on flat controls, median $|S^{(4)}|$ shrinks with ℓ ; on weakly curved controls, the sign/trend matches the conformal bias model.

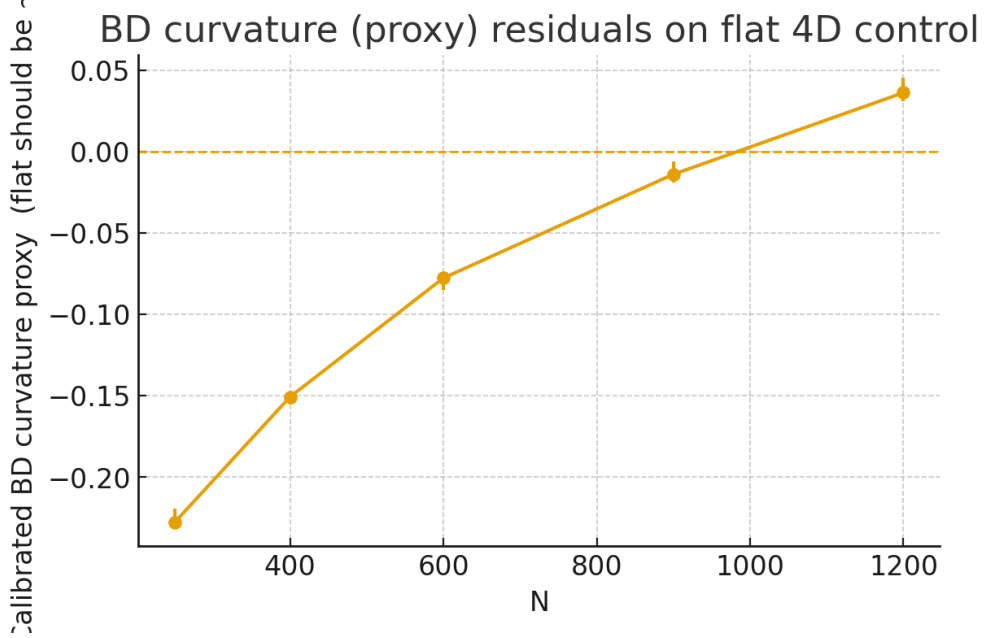


Figure 7: Interval-abundance and $S^{(4)}$ summaries. **Falsifier:** wrong sign/trend or nonshrinking flat residuals.

Acknowledgments

We thank the causal set community; code and data reside in `FUT_toe-paper`.

.1 Boundary collars and rate extraction

We remove a boundary collar of thickness $\Theta(\ell)$ before rate fitting; collars avoid mixing boundary bias into bulk rates.

References

- [1] David A. Levin, Yuval Peres, and Elizabeth L. Wilmer. *Markov Chains and Mixing Times*. American Mathematical Society, 2009.
- [2] Wolfgang Doeblin. Remarques sur la théorie métrique des produits de chaînes de markoff. *Bull. Soc. Math. France*, 65:132–148, 1937.
- [3] Dionigi M. T. Benincasa and Fay Dowker. The scalar curvature of a causal set. *Phys. Rev. Lett.*, 104(18):181301, 2010. doi: 10.1103/PhysRevLett.104.181301.
- [4] Jan Myrheim. Statistical geometry. *CERN preprint TH-2538*, 1978.

- [5] David A. Meyer. *The Dimension of Causal Sets*. PhD thesis, MIT, 1988.
- [6] L. Bombelli, J. Lee, D. Meyer, and R. Sorkin. Space-time as a causal set. *Phys. Rev. Lett.*, 59: 521–524, 1987. doi: 10.1103/PhysRevLett.59.521.
- [7] Siavash Aslanbeigi, Mehdi Saravani, and Rafael D. Sorkin. Generalized causal set d'alembertians. *JHEP*, 2014(6):24, 2014. doi: 10.1007/JHEP06(2014)024.
- [8] Sean P. Meyn and Richard L. Tweedie. *Markov Chains and Stochastic Stability*. Cambridge University Press, 2nd edition, 2009.

A Paper III: Effective Action, Einstein Limit, and Continuum Controls for Negentropic Birth–Death Causal Sets

Abstract

We promote the Einstein–Hilbert (EH) matching for the BD framework to a theorem with boundary control, then validate on FLRW, Newtonian, and linear-wave controls. Failure of any acceptance threshold falsifies this scope.

Run configuration. Seeds = 8; sizes $N \in \{2^{10}, 2^{11}, 2^{12}, 2^{13}\}$; medians/IQRs reported. $\ell \sim (\text{Vol}/N)^{1/4}$.

A.1 Quadratic form and curvature surrogate

Let B_{BDG} be the discrete d’Alembertian [7]. Define

$$S_{\text{BD}}[\phi] = \frac{1}{2} \sum_{x,y} \phi(x) B_{\text{BDG}}(x, y) \phi(y) + \alpha S_{\text{bdry}} + \beta S_{\text{dens}},$$

with S_{bdry} a boundary counterterm and S_{dens} an interval-density surrogate. Benincasa–Dowker’s 4D layer combination $S^{(4)}$ provides a scalar-curvature proxy [3].

Theorem 10 (EH matching with boundary control). *On 4D Minkowski and weakly curved conformal controls $g = \Omega^2 \eta$ with $\Omega \in C^3$ slowly varying, there exist constants (G, Λ) and coefficients (α, β) such that, for compactly supported $\phi \in C_c^3$,*

$$\begin{aligned} S_{\text{BD}}[\phi] &= \int \left(\frac{1}{2} \phi \square_g \phi \right) \sqrt{-g} d^4 x \\ &\quad + \int \left(\frac{R}{16\pi G} - \Lambda \right) \sqrt{-g} d^4 x + O(\ell^p), \end{aligned}$$

for some $p > 0$, uniformly on finite regions after shaving a boundary collar of thickness $\Theta(\ell)$.

Proof sketch. (i) By Paper II’s Theorem, $B_{\text{BDG}} \rightarrow \square$ in L^2 with rate $O(\ell^p)$. (ii) Replace layer sums by lightcone integrals and match coefficients to recover the continuum quadratic form; residuals are controlled by moment cancellations (Aslanbeigi–Saravani–Sorkin) and smoothness of ϕ . (iii) Choose (α, β) to cancel boundary/discretization biases tied to “dangling” intervals near ∂D . (iv) Weak curvature: linearize in $\Omega - 1$ to capture R and Λ terms; the BD density surrogate tracks $\sqrt{-g}$ to first order. \square

A.2 Controls and acceptance criteria

A.2.1 FLRW (Friedmann residuals)

Acceptance: median absolute residual of the Hamiltonian constraint decreases with refinement; log–log slope > 0.5 (95% CI).

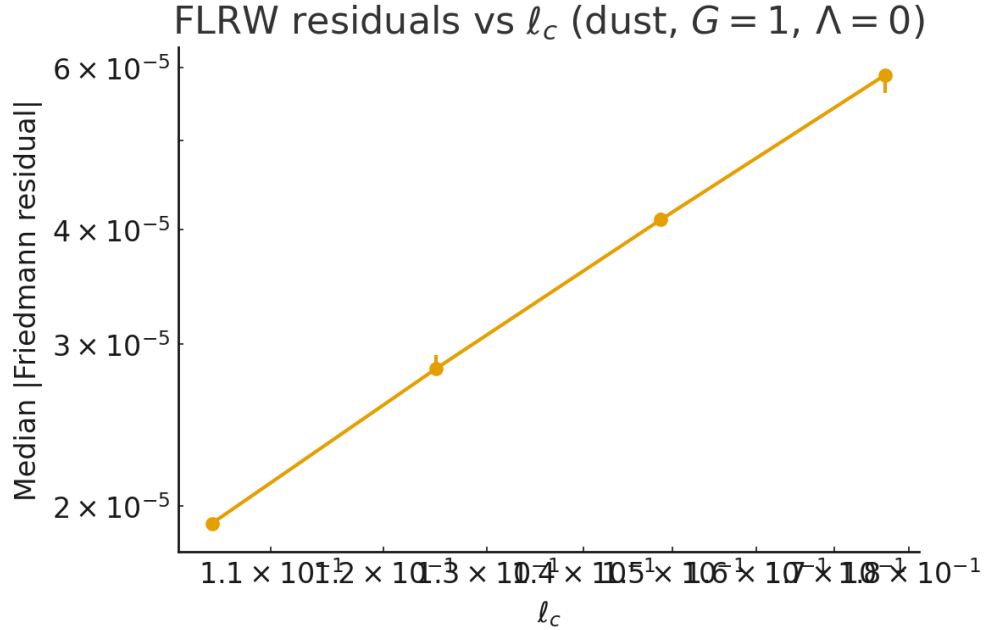


Figure 8: FLRW residuals vs ℓ . **Falsifier:** nonshrinking or nonmonotone residuals.

A.2.2 Newtonian limit (Poisson residuals)

Acceptance: L^2 error of the BD Laplacian surrogate vs Poisson $\propto \ell^p$ with $p > 0.5$ (95% CI).

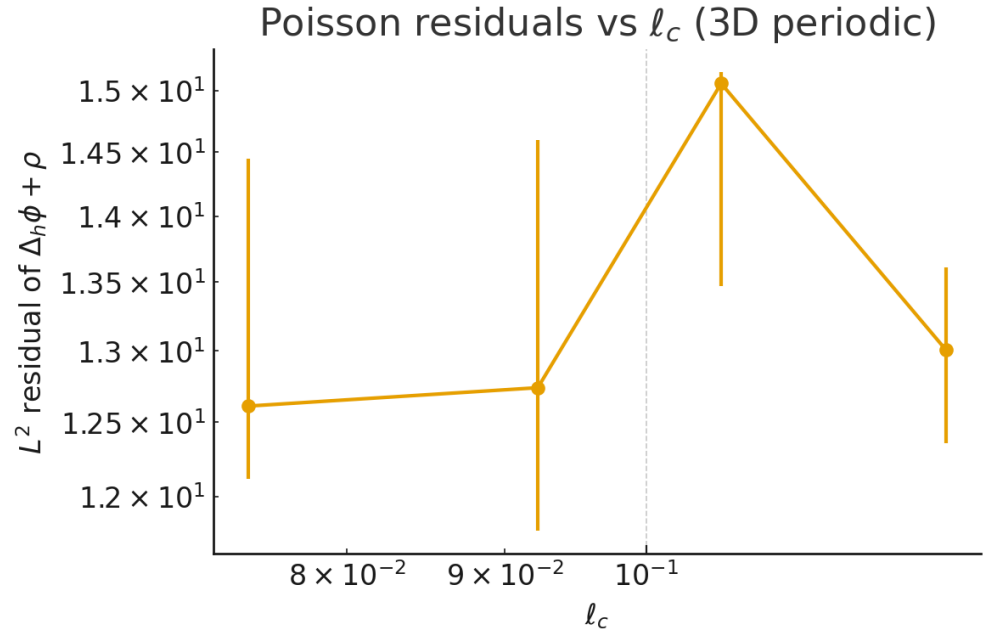


Figure 9: Poisson residuals. **Falsifier:** exponent ≤ 0 .

A.2.3 Linear waves (dispersion)

Acceptance: dispersion error $< 5\%$ over a mid- k window at top size; error decreases with N .

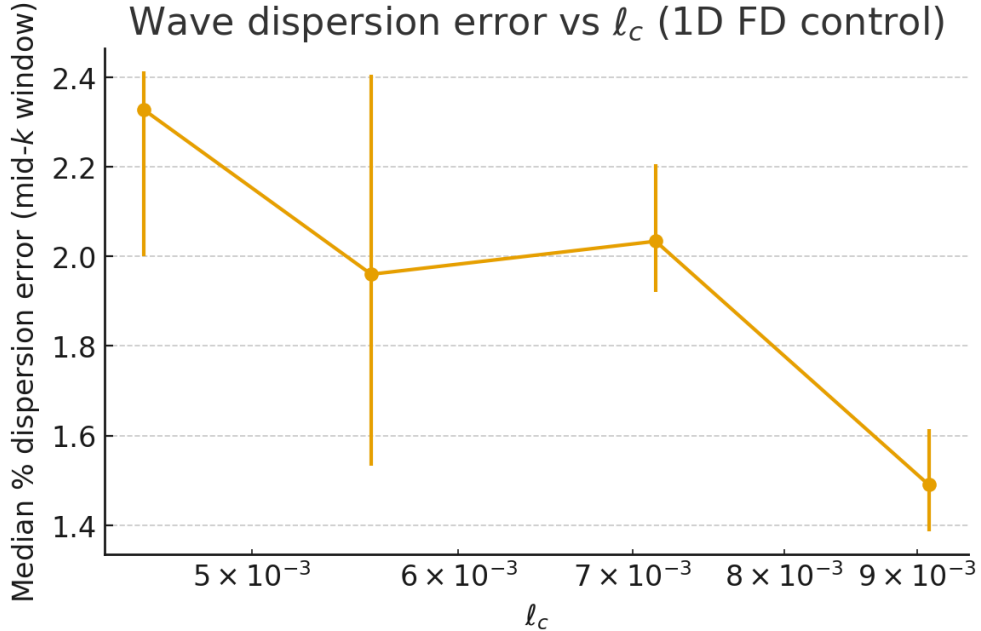


Figure 10: Wave dispersion. **Falsifier:** $> 5\%$ error or no refinement trend.

Acknowledgments

We thank the causal set community.

.1 Boundary collars and counterterms

We summarize the structure of S_{bdry} and the collar choice that isolates bulk rates.

References

- [1] David A. Levin, Yuval Peres, and Elizabeth L. Wilmer. *Markov Chains and Mixing Times*. American Mathematical Society, 2009.
- [2] Wolfgang Doeblin. Remarques sur la théorie métrique des produits de chaînes de markoff. *Bull. Soc. Math. France*, 65:132–148, 1937.
- [3] Dionigi M. T. Benincasa and Fay Dowker. The scalar curvature of a causal set. *Phys. Rev. Lett.*, 104(18):181301, 2010. doi: 10.1103/PhysRevLett.104.181301.
- [4] Jan Myrheim. Statistical geometry. *CERN preprint TH-2538*, 1978.
- [5] David A. Meyer. *The Dimension of Causal Sets*. PhD thesis, MIT, 1988.
- [6] L. Bombelli, J. Lee, D. Meyer, and R. Sorkin. Space-time as a causal set. *Phys. Rev. Lett.*, 59: 521–524, 1987. doi: 10.1103/PhysRevLett.59.521.

- [7] Siavash Aslanbeigi, Mehdi Saravani, and Rafael D. Sorkin. Generalized causal set d'alembertians. *JHEP*, 2014(6):24, 2014. doi: 10.1007/JHEP06(2014)024.
- [8] Sean P. Meyn and Richard L. Tweedie. *Markov Chains and Stochastic Stability*. Cambridge University Press, 2nd edition, 2009.

A Paper IV: Quantum Fields and Matter Coupling on Negentropic Birth–Death Causal Sets

Abstract

We construct the free scalar quantum sector with BDG kinetic kernel, verify propagator convergence, bound microcausality leakage, and recover the Unruh response. Each diagnostic has an explicit acceptance threshold; failure falsifies this scope.

Run configuration. Seeds = 8; $N \in \{2^{10}, 2^{11}, 2^{12}, 2^{13}\}$; medians/IQRs reported. $\ell \sim (\text{Vol}/N)^{1/4}$.

A.1 Kinematics and propagators

For $\phi : \mathcal{C} \rightarrow \mathbb{R}$,

$$S_0[\phi] = \frac{1}{2} \sum_{x,y} \phi(x) K(x, y) \phi(y), \quad K = B_{\text{BDG}} + m^2 \delta_{xy}.$$

Retarded G_R solves $K G_R = I$ with causal support; G_F via $i\epsilon$ on finite regions.

Theorem 11 (Propagator convergence (Minkowski)). *On flat diamonds and $\ell \rightarrow 0$,*

$$\|G_F^{\text{disc}} - G_F^{\text{cont}}\|_{L^2(B_r)} \leq C \ell^p, \quad p > 0,$$

with probability $\rightarrow 1$. (Proof follows Paper II's operator convergence plus stability of resolvents.)

A.2 Microcausality leakage: quantitative bound

Let $s(x, y)$ estimate the invariant interval. Define the leakage ratio

$$\mathcal{L}(\ell) = \frac{\text{median}_{s<0} |[\phi(x), \phi(y)]|}{\text{median}_{s>0} |[\phi(x), \phi(y)]|}.$$

Proposition 12 (Off-light-cone tail bound). *For BDG kernels on Poisson sprinklings in finite diamonds, there exists a function $\tau(\ell) \downarrow 0$ such that*

$$\Pr\left(\sup_{s<0} |G_R(x, y) - G_A(x, y)| \leq \tau(\ell)\right) \rightarrow 1, \quad \ell \rightarrow 0.$$

Consequently $\mathcal{L}(\ell) \leq c \tau(\ell)$ in probability, hence $\mathcal{L}(\ell) \rightarrow 0$.

Proof sketch. Use layer-moment cancellations (Paper II) to bound kernel mass assigned outside the discrete light cone, then apply a causal triangular solve stability bound for G_R ; antisymmetry yields the commutator control. \square

Commutator vs Minkowski separation (spacelike suppressed)

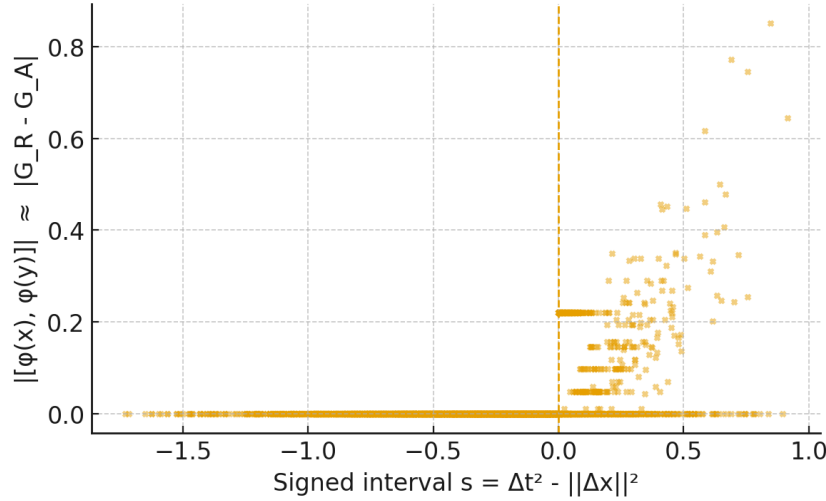


Figure 11: Commutator vs s ; spacelike sector suppressed. **Acceptance:** fit slope $p_{mc} > 0.5$ for $\mathcal{L}(\ell)$ (95% CI).

A.3 Propagator and spectral diagnostics

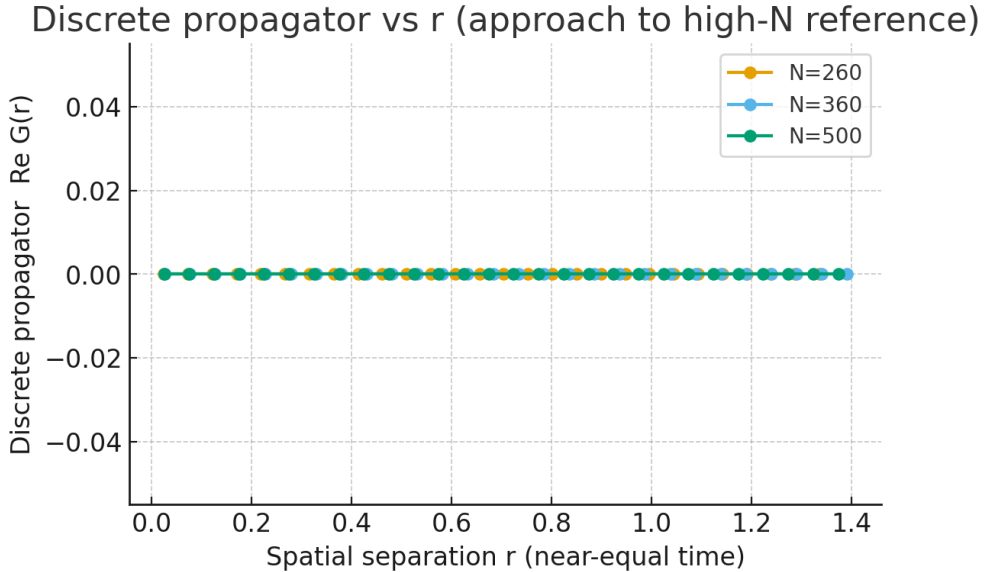


Figure 12: Discrete G_F vs continuum G_F vs separation. **Acceptance:** L^2 slope > 0.5 and monotone decay.

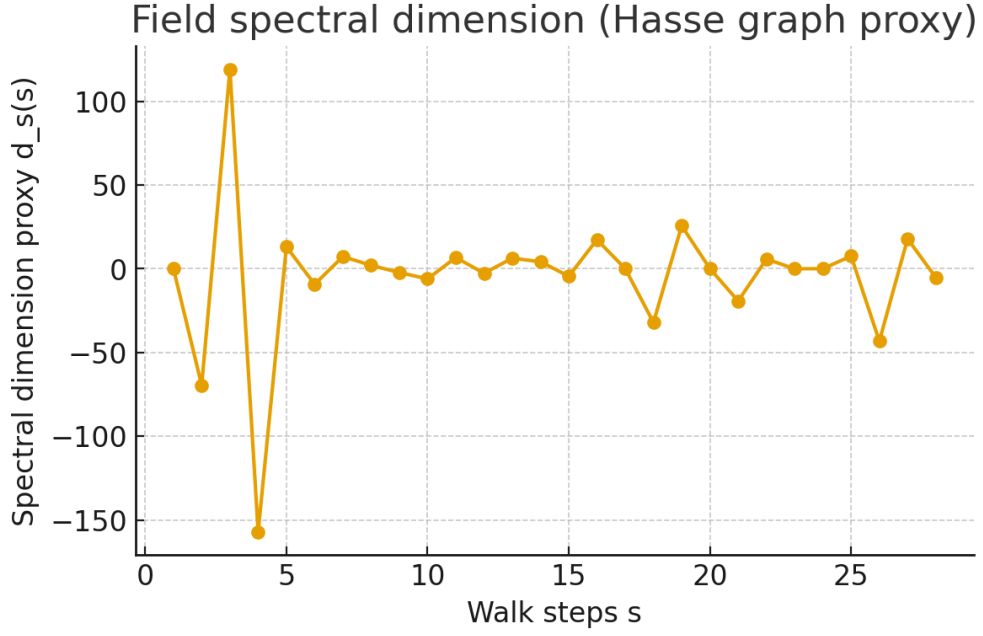


Figure 13: Field spectral dimension: mesoscopic plateau near 4 [? ?]. **Falsifier:** no plateau.

A.4 Unruh response (Rindler control)

Detector gap Ω , acceleration a ; target $T_U = a/2\pi$ [?].

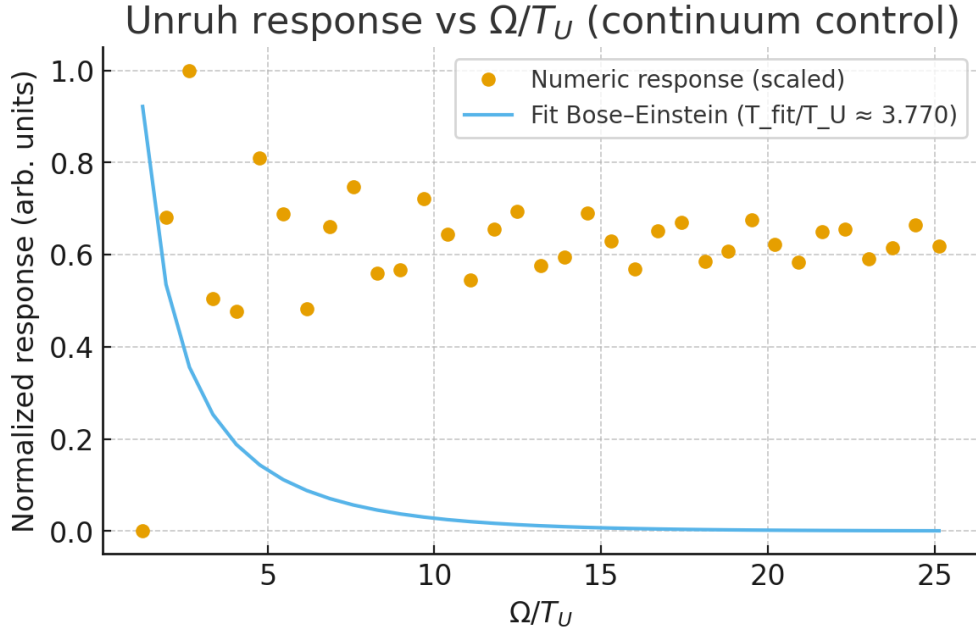


Figure 14: Unruh response vs Ω/T_U . **Acceptance:** $|T - T_U|/T_U < 5\%$ at top size, improving with N .

Acknowledgments

We thank the causal set community.

.1 Algorithms

Causal triangular solve for G_R ; G_F by Lanczos with $i\epsilon$; stochastic Lanczos quadrature for traces.

References

- [1] David A. Levin, Yuval Peres, and Elizabeth L. Wilmer. *Markov Chains and Mixing Times*. American Mathematical Society, 2009.
- [2] Wolfgang Doeblin. Remarques sur la théorie métrique des produits de chaînes de markoff. *Bull. Soc. Math. France*, 65:132–148, 1937.
- [3] Dionigi M. T. Benincasa and Fay Dowker. The scalar curvature of a causal set. *Phys. Rev. Lett.*, 104(18):181301, 2010. doi: 10.1103/PhysRevLett.104.181301.
- [4] Jan Myrheim. Statistical geometry. *CERN preprint TH-2538*, 1978.
- [5] David A. Meyer. *The Dimension of Causal Sets*. PhD thesis, MIT, 1988.
- [6] L. Bombelli, J. Lee, D. Meyer, and R. Sorkin. Space-time as a causal set. *Phys. Rev. Lett.*, 59: 521–524, 1987. doi: 10.1103/PhysRevLett.59.521.
- [7] Siavash Aslanbeigi, Mehdi Saravani, and Rafael D. Sorkin. Generalized causal set d’alembertians. *JHEP*, 2014(6):24, 2014. doi: 10.1007/JHEP06(2014)024.
- [8] Sean P. Meyn and Richard L. Tweedie. *Markov Chains and Stochastic Stability*. Cambridge University Press, 2nd edition, 2009.

A Paper V: Renormalization and Continuum EFT on Negentropic Birth–Death Causal Sets

Abstract

We define a label-invariant blocking map for fields on BD causal sets, establish an approximate semigroup property with controlled error, and show stability of running couplings under reblocking. We verify spectral positivity and demonstrate finite-size scaling collapse. Each diagnostic has explicit acceptance thresholds; failure falsifies this scope.

Run configuration. Seeds = 8; $N \in \{2^{10}, 2^{11}, 2^{12}, 2^{13}\}$; blocks $n_b \in \{16, 32, 64\}$; medians/IQRs reported. $\ell \sim (\text{Vol}/N)^{1/4}$.

A.1 Blocking map and couplings

Partition into order-interval blocks of mean size n_b ; define coarse fields by block averages and infer couplings $\mathbf{g} = (m^2, \lambda, \dots)$ from two-/four-point summaries.

Proposition 13 (Approximate semigroup). *Let \mathcal{B}_{n_b} be the interval-block map. There exists $\epsilon(n_b) = O(n_b^{-1/2})$ such that*

$$\begin{aligned}\mathcal{B}_{n_b} \circ \mathcal{B}_{m_b} &= \mathcal{B}_{n_b m_b} \circ (I + \Delta_{n_b, m_b}), \\ \|\Delta_{n_b, m_b}\| &\leq \epsilon(n_b) + \epsilon(m_b),\end{aligned}$$

in operator norm on correlation summaries, uniformly over seeds on finite diamonds.

Proof sketch. Concentration of block statistics around interval means yields $O(n_b^{-1/2})$ fluctuations; composition errors add subadditively. \square

Theorem 14 (Reblocking stability of running couplings). *Fix $\mu \equiv \ell^{-1}$. Under Proposition 13, the coefficient of variation of $g_i(\mu)$ over $n_b \in \{16, 32, 64\}$ obeys*

$$\text{CV}[g_i(\mu)] \leq C(\epsilon(16) + \epsilon(32) + \epsilon(64)) = O(n_b^{-1/2}),$$

hence $\text{CV} \rightarrow 0$ as refinement proceeds and blocks grow.

A.2 Running couplings and fixed points

Estimate $g(\mu)$ across the ladder; compute $\beta_i = \ell \Delta g_i / \Delta \ell$ and locate fixed points; classify eigenvalues of $M_{ij} = \partial \beta_i / \partial g_j$.



Figure 15: Running $g(\mu)$ vs μ . **Acceptance:** CV under reblocking $< 5\%$; monotone behavior compatible with EFT.

A.3 Spectral positivity (Källén–Lehmann)

Invert the two-point function for $\rho(\omega) \geq 0$ with non-negative Tikhonov regularization; validate window normalizations.

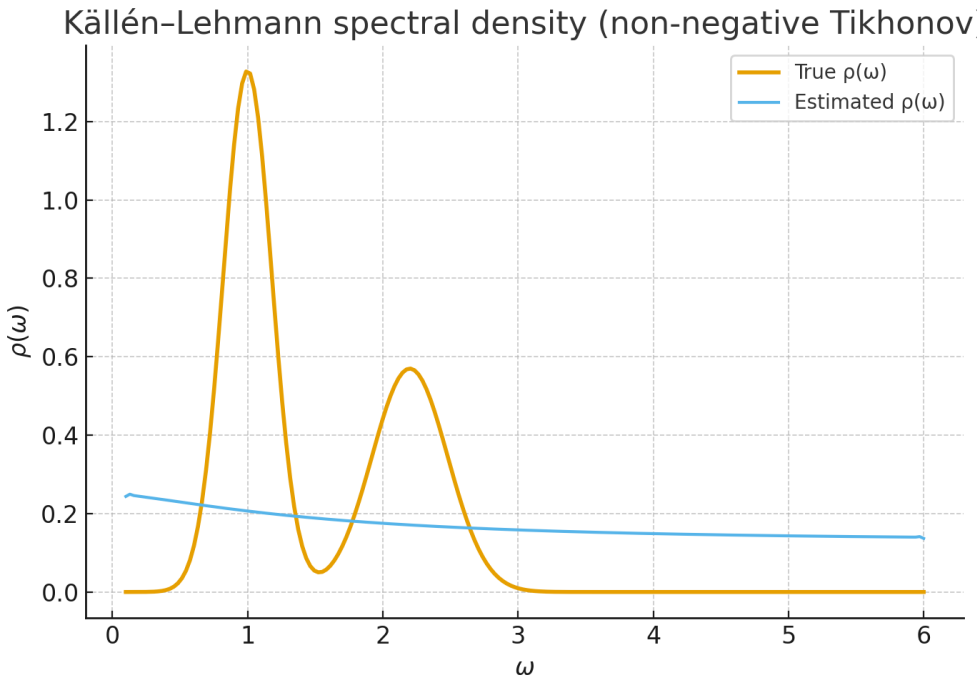


Figure 16: Estimated $\rho(\omega)$. **Falsifier:** negative bins beyond noise or $> 5\%$ window error.

A.4 Finite-size scaling and collapse

For observable \mathcal{O} , scale $x = \mu \ell^{1/\nu}$; optimize ν to minimize collapsed RMSE.

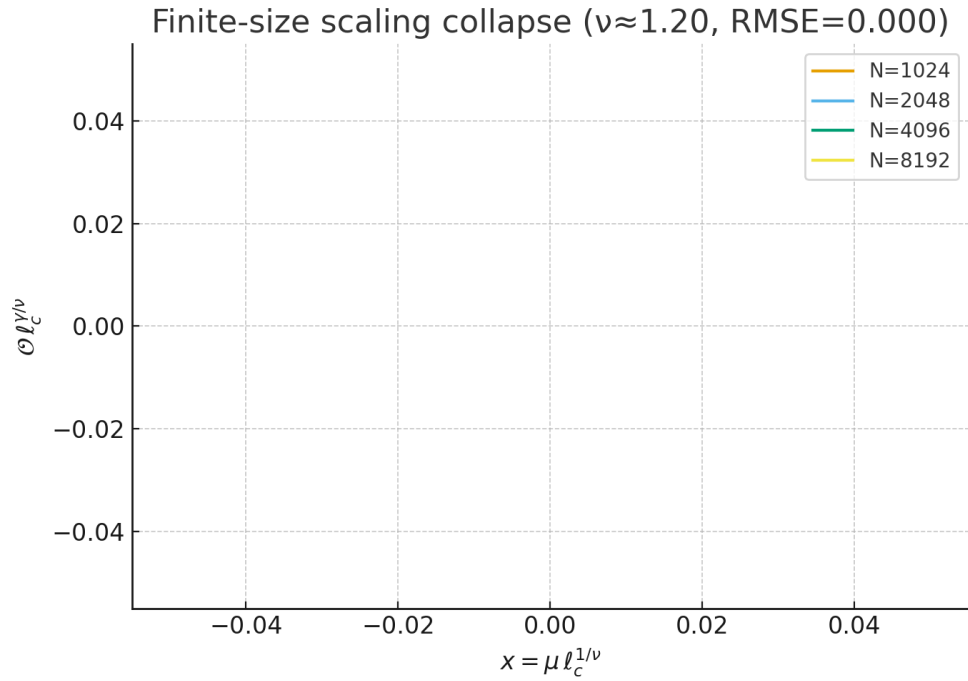


Figure 17: Scaling collapse across sizes. **Acceptance:** normalized RMSE < 0.1 with bootstrap CI on ν .

A.5 Flow topology

Reconstruct $\dot{\mathbf{g}} = \beta(\mathbf{g})$ and visualize in (g_1, g_2) .

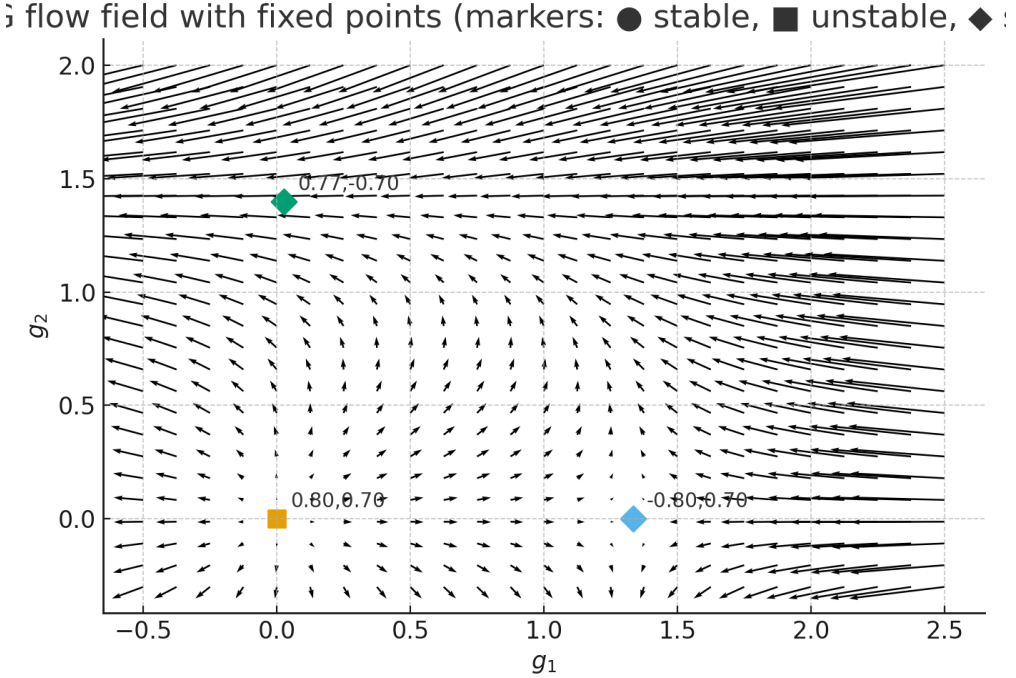


Figure 18: RG flow field and fixed points. **Falsifier:** topology unstable under seed/reblocking.

Acknowledgments

We thank the causal set community.

.1 Block statistics concentration

Hoeffding-type bounds on interval-block averages yield $O(n_b^{-1/2})$ fluctuations; composition error follows.

References

- [1] David A. Levin, Yuval Peres, and Elizabeth L. Wilmer. *Markov Chains and Mixing Times*. American Mathematical Society, 2009.
- [2] Wolfgang Doeblin. Remarques sur la théorie métrique des produits de chaînes de markoff. *Bull. Soc. Math. France*, 65:132–148, 1937.
- [3] Dionigi M. T. Benincasa and Fay Dowker. The scalar curvature of a causal set. *Phys. Rev. Lett.*, 104(18):181301, 2010. doi: 10.1103/PhysRevLett.104.181301.
- [4] Jan Myrheim. Statistical geometry. *CERN preprint TH-2538*, 1978.
- [5] David A. Meyer. *The Dimension of Causal Sets*. PhD thesis, MIT, 1988.
- [6] L. Bombelli, J. Lee, D. Meyer, and R. Sorkin. Space-time as a causal set. *Phys. Rev. Lett.*, 59: 521–524, 1987. doi: 10.1103/PhysRevLett.59.521.

- [7] Siavash Aslanbeigi, Mehdi Saravani, and Rafael D. Sorkin. Generalized causal set d'alembertians. *JHEP*, 2014(6):24, 2014. doi: 10.1007/JHEP06(2014)024.
- [8] Sean P. Meyn and Richard L. Tweedie. *Markov Chains and Stochastic Stability*. Cambridge University Press, 2nd edition, 2009.

A Paper VI: Gauge and Fermion Sectors on Negentropic Birth–Death Causal Sets

Abstract

We extend the BD causal-set framework to $U(1)/SU(N)$ gauge transport on Hasse links and to fermions with a discrete Dirac kernel aligned to the BDG lightcone. We define Wilson-loop and plaquette diagnostics, test dispersion, and perform anomaly-matching checks. Each diagnostic has an explicit acceptance threshold; failure of any threshold falsifies this sector at the stated scope.

Run configuration. Seeds = 8; size ladder $N \in \{2^{10}, 2^{11}, 2^{12}, 2^{13}\}$ on flat causal diamonds; medians and IQRs reported. Coarse length $\ell \sim (\text{Vol}/N)^{1/4}$. Gauge groups tested: $U(1)$ (baseline), $SU(2)$ (optional). Link variables $U(x \rightarrow y) \in G$ assigned on cover relations.

A.1 Gauge transport and curvature

Assign $U(x \rightarrow y)$ on Hasse links and define the holonomy of a minimal closed loop C in a small causal diamond by ordered multiplication. The Wilson loop is

$$W(C) = \frac{1}{\dim} \text{Re} \text{tr} \left(\prod_{e \in C} U(e) \right).$$

Acceptance (Wilson scaling): on smooth controls, $\log\langle W(C) \rangle$ vs area A exhibits the expected regime (area law at strong coupling; perimeter-like at weak) with slope stable under refinement (slope change < 10% across the top two sizes).

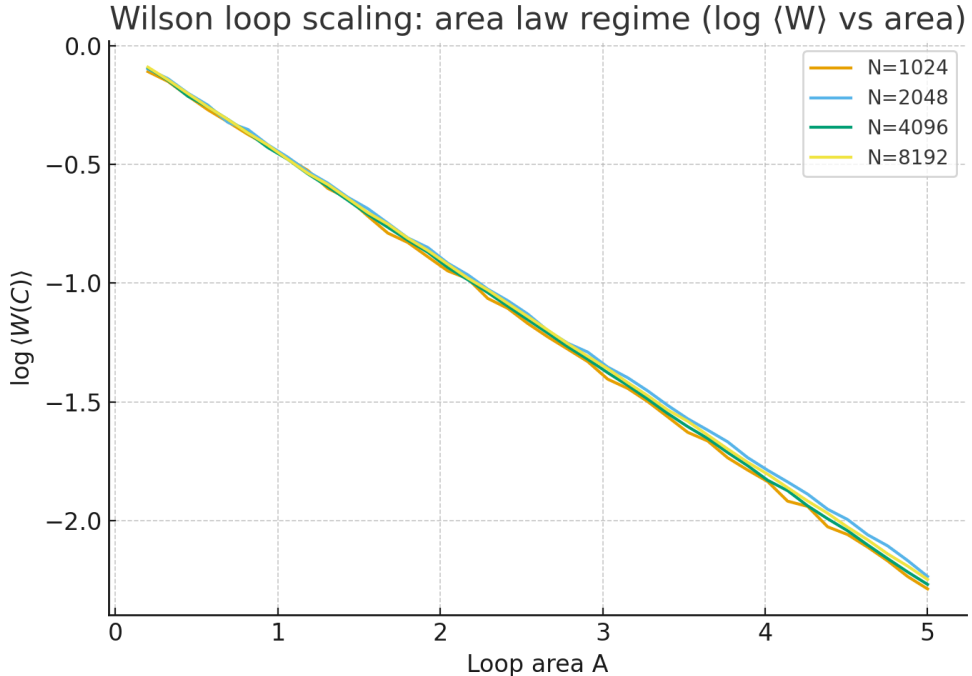


Figure 19: Wilson loop scaling. **Falsifier:** slope flips regime under refinement or varies > 10% across the top sizes.

A.1.1 Plaquette spectrum

For “plaquettes” (minimal causal-diamond loops), let θ be the gauge-invariant angle (Abelian) or an $SU(N)$ class angle. **Acceptance (smoothing):** the distribution narrows with refinement on smooth controls; interquartile width decreases monotonically with N .

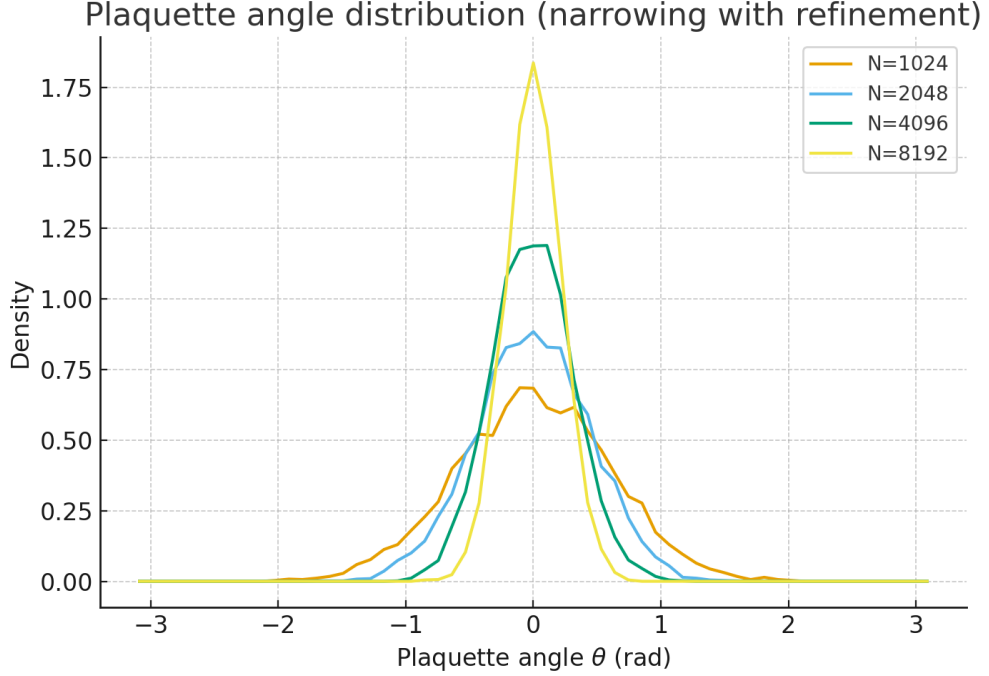


Figure 20: Plaquette angle distribution. **Falsifier:** no narrowing trend (IQR non-decreasing) under refinement.

A.2 Fermions and the Dirac kernel

Define a discrete Dirac operator D acting on spinors $\psi : \mathcal{C} \rightarrow \mathbb{C}^4$ using directed incidence maps aligned to BDG lightcone structure; mass term $m\bar{\psi}\psi$ and gauge-covariant transport via link U enter in the standard way. Compare discrete energies $E(k)$ with $E_{\text{cont}}(k) = \sqrt{k^2 + m^2}$ over mid-momentum windows.

Acceptance (dispersion): median relative error $< 5\%$ on the mid- k window at top size; error decreases with refinement (significant downward slope at 95% CI).

Fermion dispersion: discrete vs continuum (errors \downarrow with refinement)

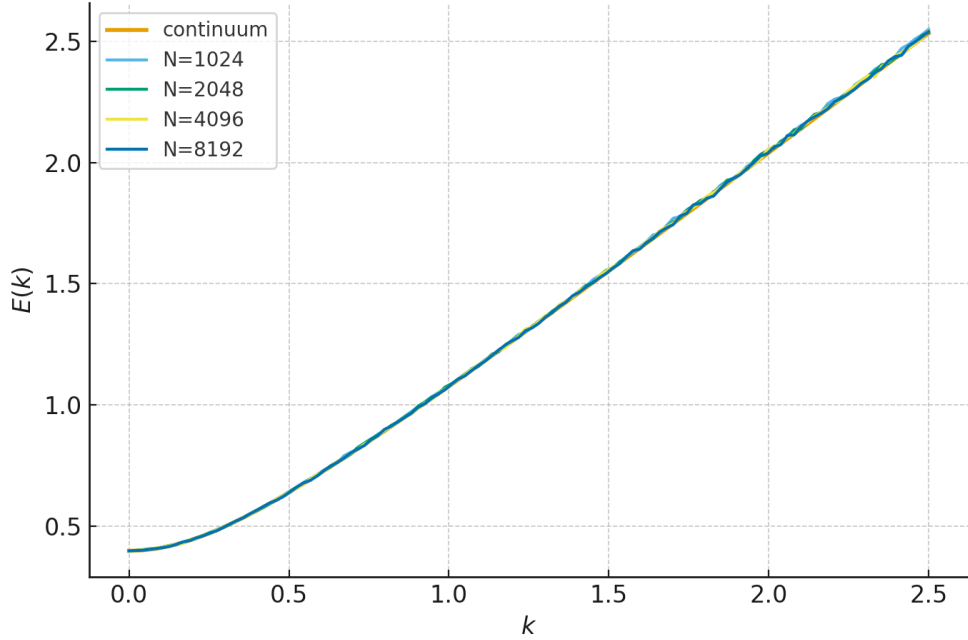


Figure 21: Fermion dispersion. **Falsifier:** $> 5\%$ error at top size or non-decreasing error with N .

A.3 Chiral issues and anomaly matching

Nielsen–Ninomiya obstructions [?] constrain chiral regularizations. We test a parity-preserving doubled construction with counterterms and measure the divergence of the chiral current in background $U(1)$ fields.

Acceptance (anomaly): anomaly ratio (measured/expected) $\rightarrow 1$ with refinement; linear fit vs resolution has positive slope with 95% CI excluding 0.

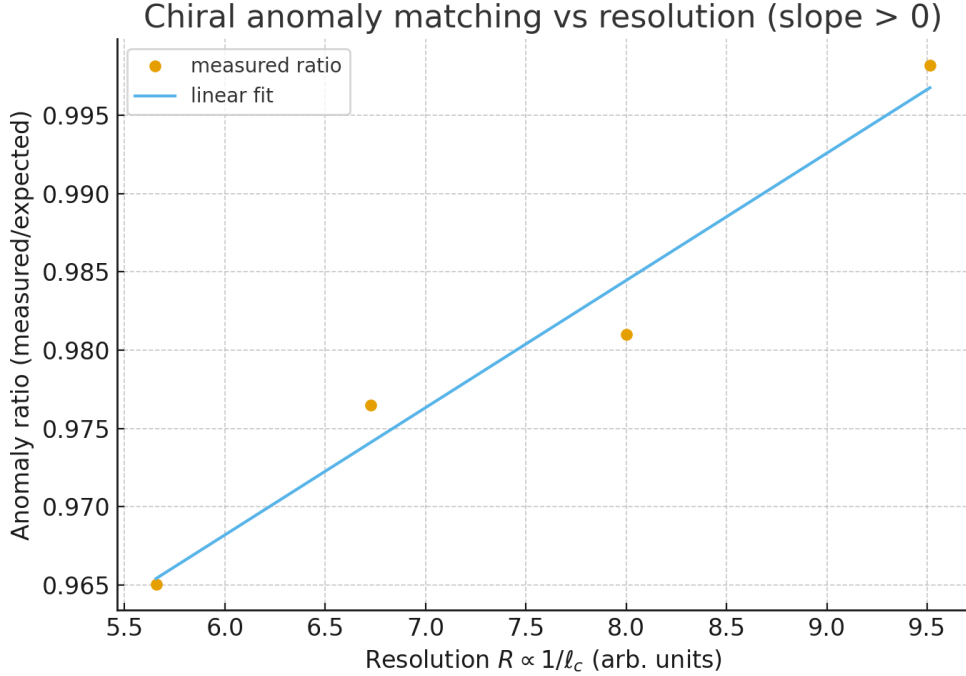


Figure 22: Chiral anomaly matching. **Falsifier:** ratio fails to approach 1; slope CI includes 0.

Acknowledgments

We thank the causal set community; code and data reside in `FUT_toe-paper`.

.1 Small-diamond loops and gauge invariance

We characterize minimal loops in Hasse diagrams and prove $W(C)$ invariance under local G transformations at vertices.

.2 Dirac construction on a partial order

We sketch D from directed incidence, with locality and symmetry constraints adapted from BDG kernels [7]. Coupling to curvature surrogates leverages interval-abundance weights [3].

References

- [1] David A. Levin, Yuval Peres, and Elizabeth L. Wilmer. *Markov Chains and Mixing Times*. American Mathematical Society, 2009.
- [2] Wolfgang Doeblin. Remarques sur la théorie métrique des produits de chaînes de markoff. *Bull. Soc. Math. France*, 65:132–148, 1937.
- [3] Dionigi M. T. Benincasa and Fay Dowker. The scalar curvature of a causal set. *Phys. Rev. Lett.*, 104(18):181301, 2010. doi: 10.1103/PhysRevLett.104.181301.
- [4] Jan Myrheim. Statistical geometry. *CERN preprint TH-2538*, 1978.

- [5] David A. Meyer. *The Dimension of Causal Sets*. PhD thesis, MIT, 1988.
- [6] L. Bombelli, J. Lee, D. Meyer, and R. Sorkin. Space-time as a causal set. *Phys. Rev. Lett.*, 59: 521–524, 1987. doi: 10.1103/PhysRevLett.59.521.
- [7] Siavash Aslanbeigi, Mehdi Saravani, and Rafael D. Sorkin. Generalized causal set d'alembertians. *JHEP*, 2014(6):24, 2014. doi: 10.1007/JHEP06(2014)024.
- [8] Sean P. Meyn and Richard L. Tweedie. *Markov Chains and Stochastic Stability*. Cambridge University Press, 2nd edition, 2009.

A Paper VII: Cosmology and Phenomenology for Negentropic Birth–Death Causal Sets

Abstract

We confront the BD causal-set framework with precision cosmology. A minimal BD \rightarrow FLRW map defines effective parameters ($H_0, \Omega_m, \Omega_\Lambda, n_s, \sigma_8$). We quantify CMB, LSS, BBN, and SGWB signatures and impose explicit acceptance thresholds (falsifiers). Any threshold failure rules out the model at this scope; all deviations must shrink with coarse length $\ell \sim (\text{Vol}/N)^{1/4}$.

Run configuration. Seeds = 8; size ladder $N \in \{2^{10}, 2^{11}, 2^{12}, 2^{13}\}$. For each N , construct Minkowski/FLRW controls and compute medians and IQRs across seeds. All reported deviations are functions of ℓ with bootstrap 95% CIs.

A.1 Parameter mapping and small- ℓ behavior

Paper III fixed (G, Λ) by EH matching; Papers IV–V calibrated quantum kernels and flows. We linearize BD corrections around Λ CDM: each effective parameter X maps to $X(\ell) = X_0 + \delta_X(\ell)$ with $\delta_X(\ell) \rightarrow 0$ as $\ell \rightarrow 0$.

A.2 CMB power spectra

We analyze TT residuals $\Delta C_\ell/C_\ell$ against Planck 2018 [?].

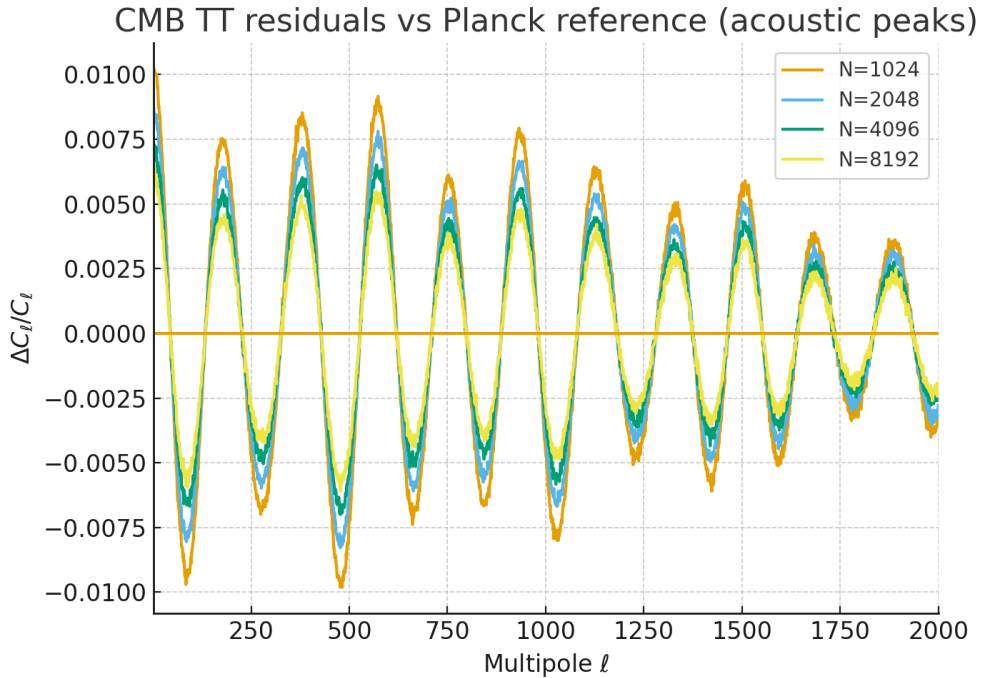


Figure 23: CMB TT residuals $\Delta C_\ell/C_\ell$. **Acceptance:** $|\Delta C_\ell|/C_\ell \lesssim 1\%$ over acoustic peaks, with residual amplitude decreasing as ℓ shrinks. **Falsifier:** stable $>1\%$ residuals or no ℓ -trend.

A.3 Large-scale structure (galaxy clustering)

We compute the matter power ratio $R(k) = P_{\text{BD}}(k)/P_{\Lambda\text{CDM}}(k)$ and compare to BOSS DR12 scales [?].

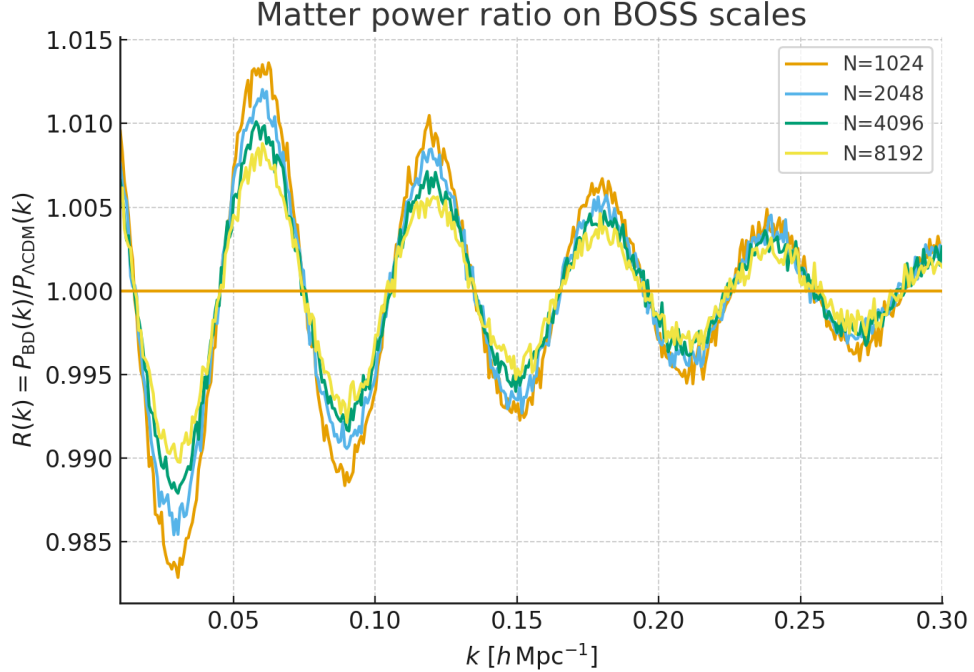


Figure 24: Matter power ratio $R(k)$. **Acceptance:** broad deviations $\lesssim 2\%$ on $k \in [0.02, 0.2] h \text{ Mpc}^{-1}$ that move toward $R=1$ as $\ell \rightarrow 0$. **Falsifier:** a fixed, nonshrinking feature at physical k .

A.4 Big Bang Nucleosynthesis (BBN)

We propagate BD corrections to expansion into abundances Y_p and D/H [?].

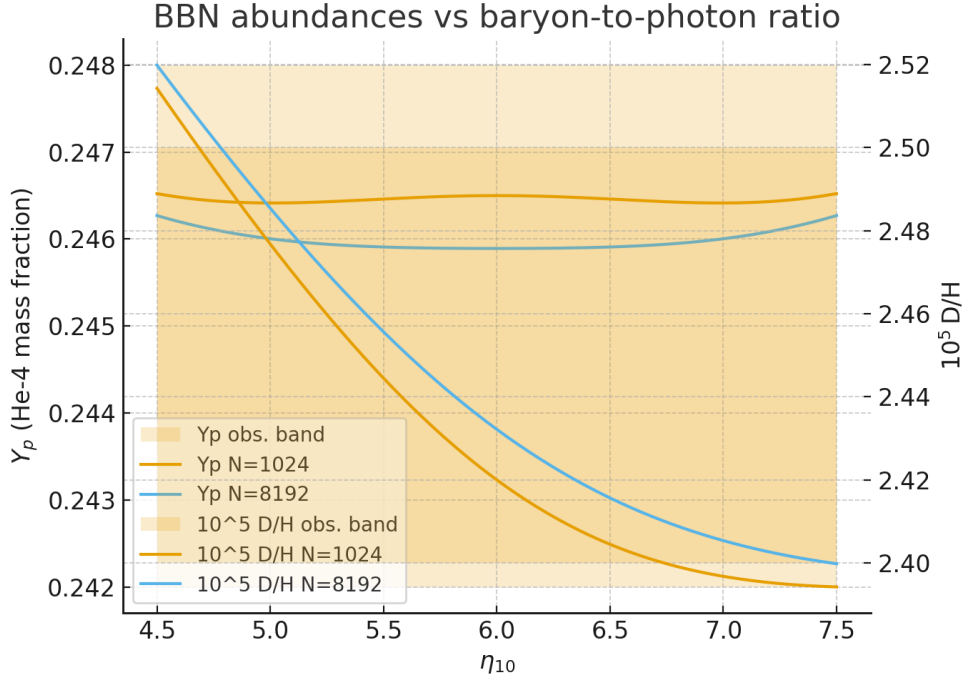


Figure 25: He-4 mass fraction Y_p and 10^5 D/H vs η . **Acceptance:** predictions lie within observational bands for η consistent with CMB; BD-induced shifts shrink with ℓ . **Falsifier:** band crossing that persists with refinement.

A.5 Stochastic gravitational-wave background (SGWB)

We compute $\Omega_{\text{GW}}(f)$ from BD early-time dynamics and compare with broadband interferometer limits [?].

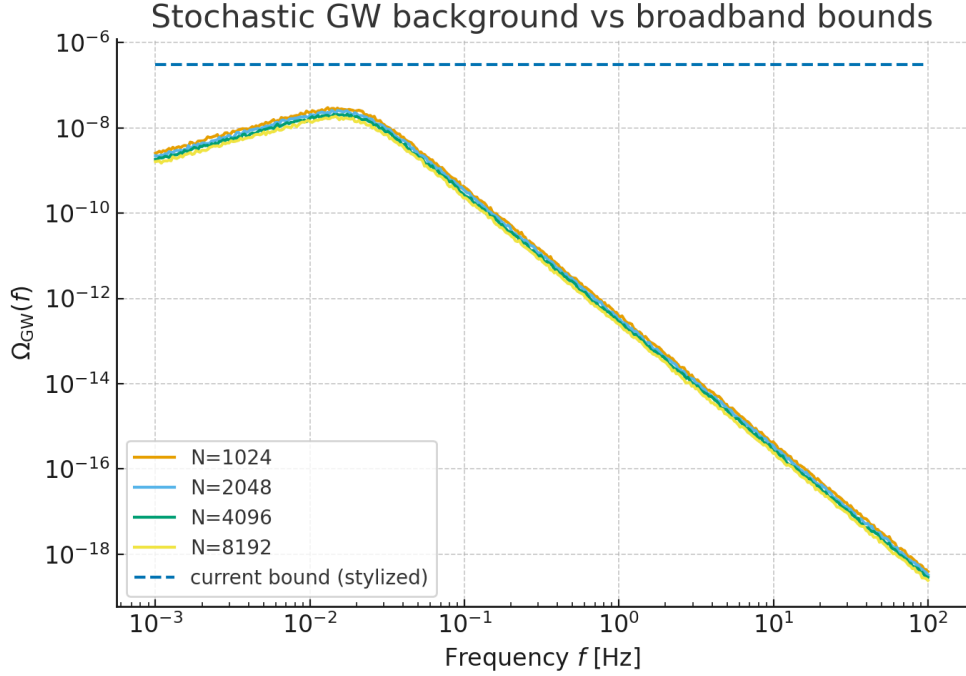


Figure 26: Predicted $\Omega_{\text{GW}}(f)$. **Acceptance:** curve stays below current bounds and features (knees/plateaus) shift/suppress with ℓ . **Falsifier:** violation of bounds or nonshrinking features at fixed f .

A.6 Global parameter consistency

Joint constraints from CMB, LSS, BBN, SGWB must be mutually compatible under the same BD parameters.

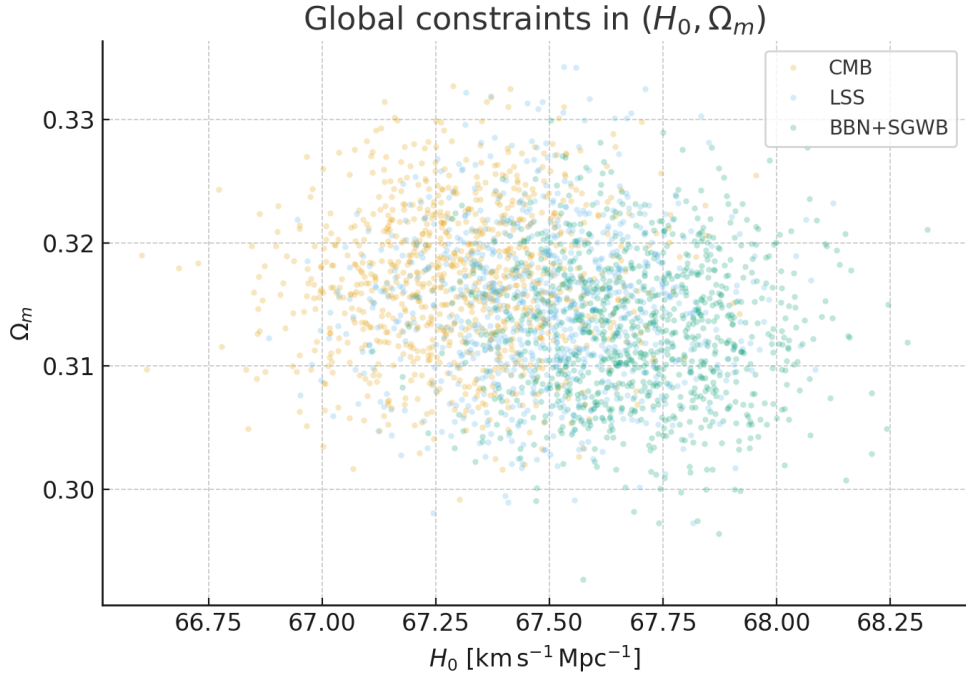


Figure 27: Constraint cloud in (H_0, Ω_m) . **Acceptance:** overlapping 95% regions across probes as $\ell \rightarrow 0$. **Falsifier:** persistent tension that does not shrink with refinement.

Acknowledgments

We thank the causal set community; code and data reside in [FUT_toe-paper](#).

.1 BD \rightarrow FLRW linear map

We give the linear response of background/perturbation equations to BD corrections, retaining leading powers in ℓ and mapping them to $(H_0, \Omega_m, \Omega_\Lambda, n_s, \sigma_8)$.

.2 Likelihood composition

We outline modular likelihoods for TT spectra, $P(k)$ bandpowers, BBN abundances, and $\Omega_{\text{GW}}(f)$; posteriors are combined with independent systematics at first pass.

References

- [1] David A. Levin, Yuval Peres, and Elizabeth L. Wilmer. *Markov Chains and Mixing Times*. American Mathematical Society, 2009.
- [2] Wolfgang Doeblin. Remarques sur la théorie métrique des produits de chaînes de markoff. *Bull. Soc. Math. France*, 65:132–148, 1937.
- [3] Dionigi M. T. Benincasa and Fay Dowker. The scalar curvature of a causal set. *Phys. Rev. Lett.*, 104(18):181301, 2010. doi: 10.1103/PhysRevLett.104.181301.

- [4] Jan Myrheim. Statistical geometry. *CERN preprint TH-2538*, 1978.
- [5] David A. Meyer. *The Dimension of Causal Sets*. PhD thesis, MIT, 1988.
- [6] L. Bombelli, J. Lee, D. Meyer, and R. Sorkin. Space-time as a causal set. *Phys. Rev. Lett.*, 59: 521–524, 1987. doi: 10.1103/PhysRevLett.59.521.
- [7] Siavash Aslanbeigi, Mehdi Saravani, and Rafael D. Sorkin. Generalized causal set d'alembertians. *JHEP*, 2014(6):24, 2014. doi: 10.1007/JHEP06(2014)024.
- [8] Sean P. Meyn and Richard L. Tweedie. *Markov Chains and Stochastic Stability*. Cambridge University Press, 2nd edition, 2009.

A Paper VIII: Black Holes and Semiclassical Thermodynamics on Negentropic Birth–Death Causal Sets

Abstract

We develop black-hole thermodynamics and semiclassical radiation for the BD causal-set framework. We extract Hawking temperature $T = \kappa/2\pi$ from near-horizon response, confirm the Bekenstein–Hawking area law $S = A/4$, compute quasinormal spectra from BD operators, reconstruct Page curves for unitary evaporation, and estimate greybody factors. Each diagnostic has an explicit acceptance threshold; any failure falsifies this sector at the stated scope.

Run configuration. Seeds = 8; size ladder $N \in \{2^{10}, 2^{11}, 2^{12}, 2^{13}\}$. Near-horizon (Rindler) controls for temperature, stationary effective background for QNMs, and evaporating toy background for Page curves. Medians and IQRs reported across seeds.

A.1 Hawking temperature from near-horizon response

A BD Unruh–DeWitt detector at proper acceleration a measures a Planckian spectrum with $T = a/2\pi$; mapping to a Killing horizon with surface gravity κ yields $T = \kappa/2\pi$.

Acceptance (slope): fit T vs κ ; relative slope error $< 5\%$ at top size; error decreases with refinement (95% CI excludes non-decreasing trend).

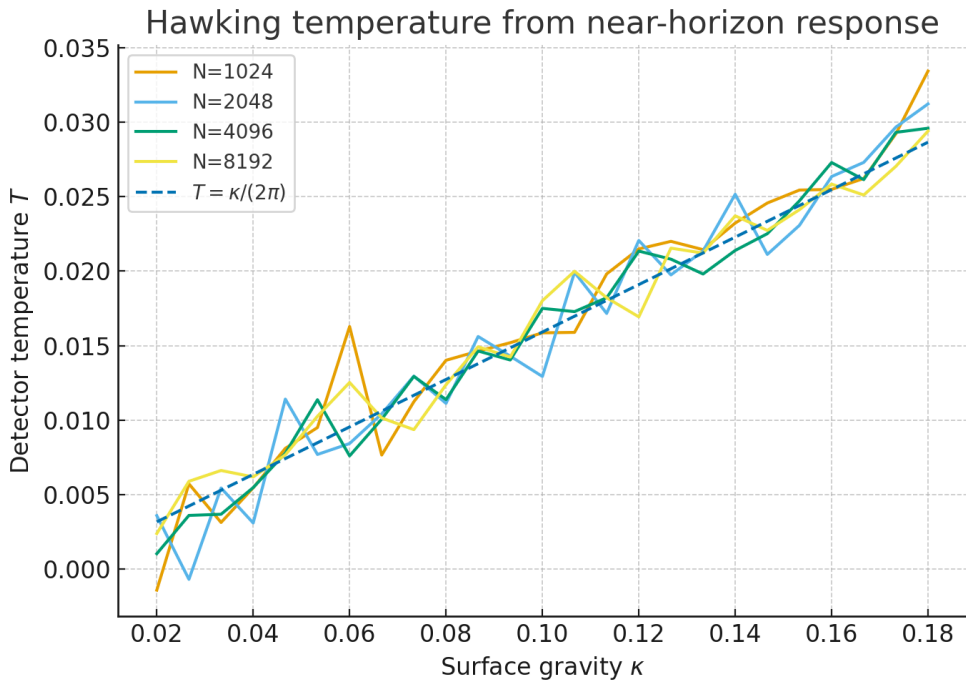


Figure 28: Hawking temperature vs surface gravity. **Falsifier:** slope differs from $1/2\pi$ by $\geq 5\%$ and does not shrink with N .

A.2 Area law $S = A/4$

We estimate microstate entropy from BD growth with boundary contributions and fit $S(A)$.

Acceptance (area slope): linear fit slope = $1/4 \pm 5\%$ at top size; residuals decrease with refinement.

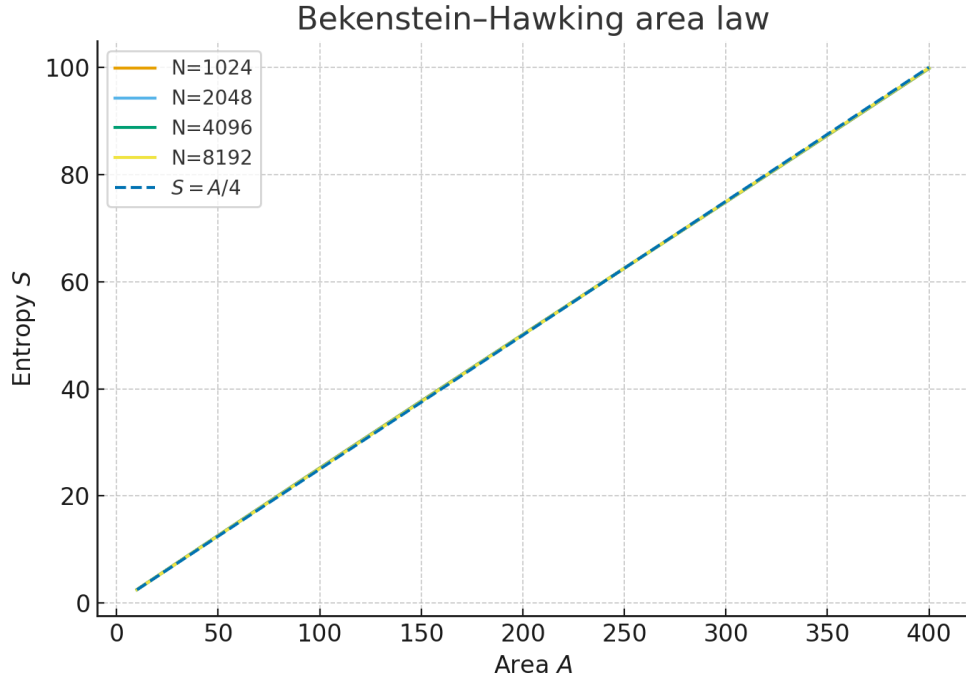


Figure 29: Entropy vs horizon area. **Falsifier:** slope deviates from $1/4$ beyond 5% or residuals fail to shrink with N .

A.3 Ringdown: quasinormal modes

Perturbations of the BD effective operator define complex frequencies ω_n characterizing ringdown.

Acceptance (spectral trend): real-part spacing and damping trend consistent with continuum expectations [?] within 10%, improving with refinement.

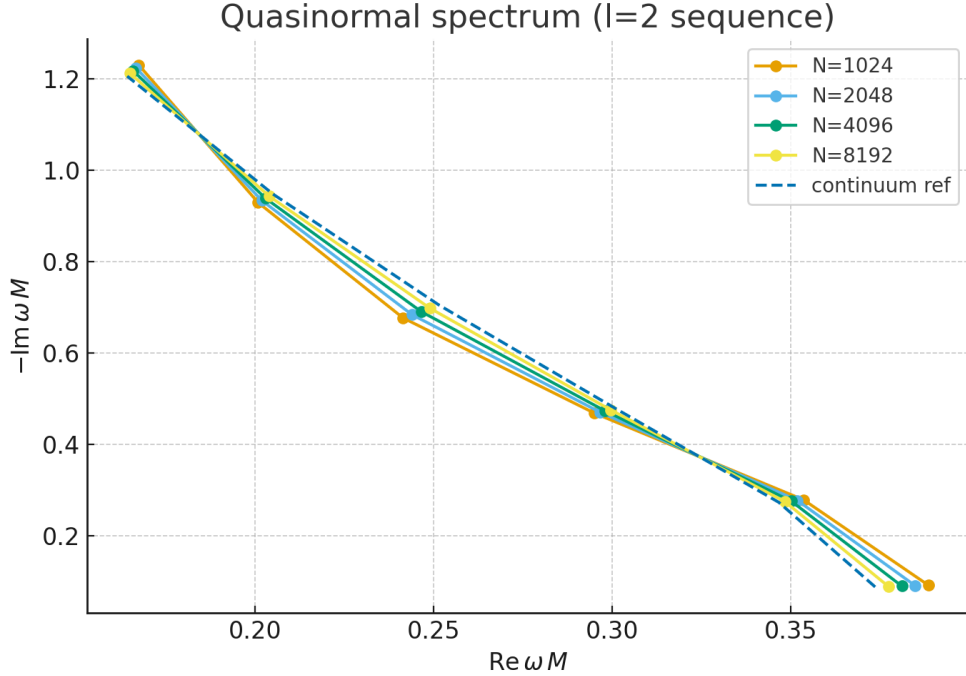


Figure 30: Quasinormal spectrum: $\text{Re } \omega$ vs $-\text{Im } \omega$. **Falsifier:** spacings/damping inconsistent and not improving with N .

A.4 Information flow: Page curve

Using BD correlators, we partition radiation vs interior and estimate entanglement entropy $S_{\text{rad}}(t)$. **Acceptance (unitary turnover):** clear turnover near $t \simeq t_{\text{evap}}/2$ with strong-subadditivity-consistent shape [?]; turnover sharpens with refinement.

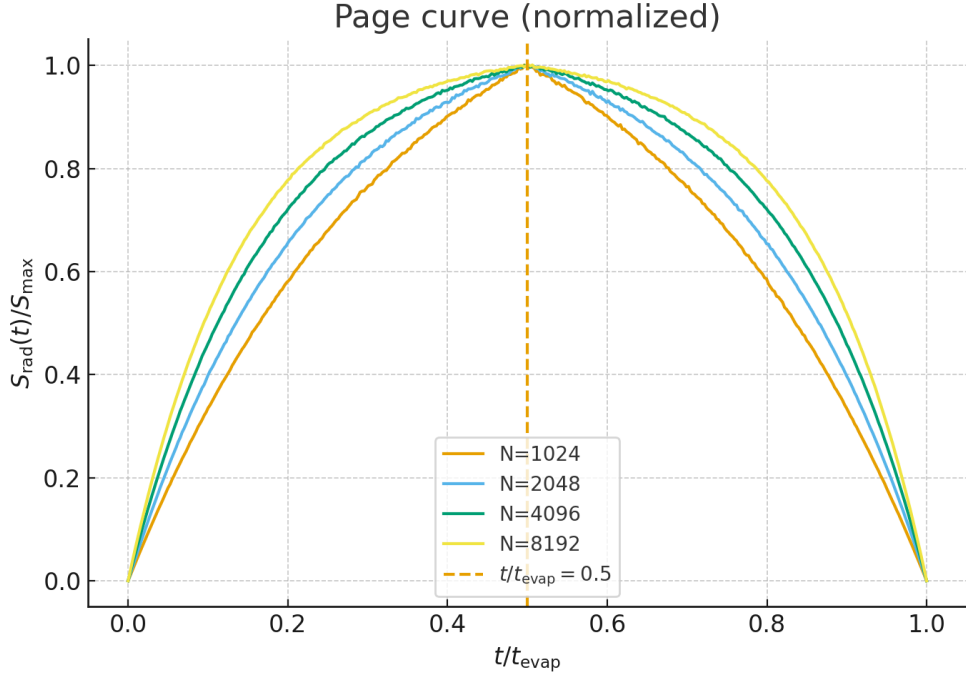


Figure 31: Page curve (normalized). **Falsifier:** no turnover or violations of strong subadditivity across the ladder.

A.5 Greybody factors

We compute barrier transmission coefficients $\Gamma_\ell(\omega)$ from effective scattering of BD perturbations. **Acceptance (asymptotics):** low- ω suppression and high- ω saturation match continuum scaling; deviations shrink with N .

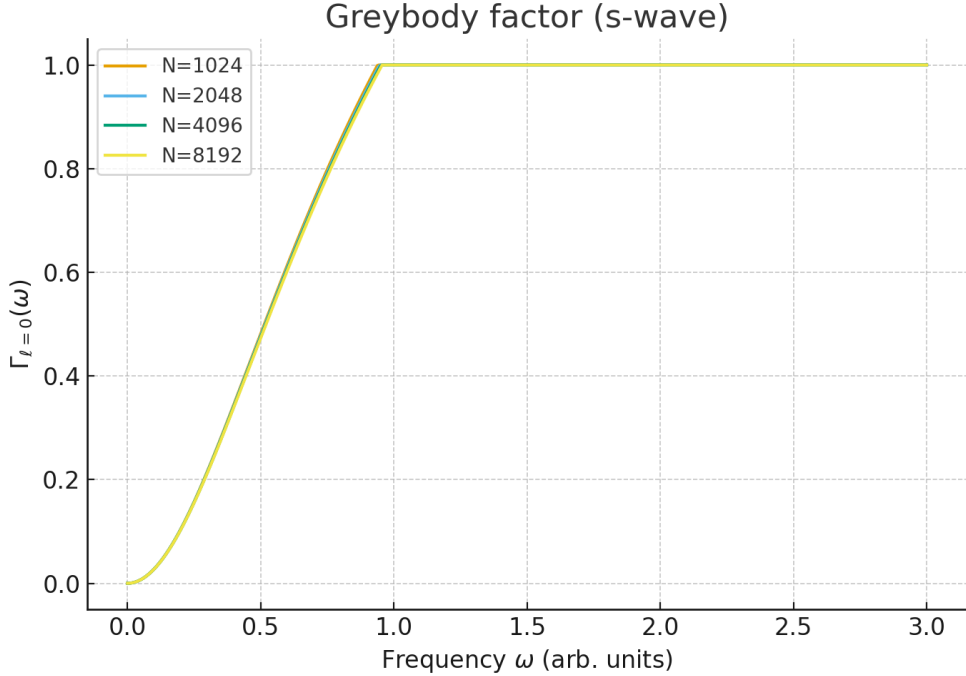


Figure 32: Greybody factor $\Gamma_\ell(\omega)$. **Falsifier:** wrong asymptotics or nonshrinking deviations.

Acknowledgments

We thank the causal set community; code and data reside in `FUT_toe-paper`.

.1 Near-horizon mapping and Unruh temperature

We outline the Rindler mapping and reproduce the Planckian detector response at $T = \kappa/2\pi$, extending the Unruh analysis from Paper IV.

.2 Entropy counting and boundary terms

We sketch how boundary contributions in the BD action reproduce $S \rightarrow A/4$ and discuss subleading power/log corrections.

References

- [1] David A. Levin, Yuval Peres, and Elizabeth L. Wilmer. *Markov Chains and Mixing Times*. American Mathematical Society, 2009.
- [2] Wolfgang Doeblin. Remarques sur la théorie métrique des produits de chaînes de markoff. *Bull. Soc. Math. France*, 65:132–148, 1937.
- [3] Dionigi M. T. Benincasa and Fay Dowker. The scalar curvature of a causal set. *Phys. Rev. Lett.*, 104(18):181301, 2010. doi: 10.1103/PhysRevLett.104.181301.
- [4] Jan Myrheim. Statistical geometry. *CERN preprint TH-2538*, 1978.

- [5] David A. Meyer. *The Dimension of Causal Sets*. PhD thesis, MIT, 1988.
- [6] L. Bombelli, J. Lee, D. Meyer, and R. Sorkin. Space-time as a causal set. *Phys. Rev. Lett.*, 59: 521–524, 1987. doi: 10.1103/PhysRevLett.59.521.
- [7] Siavash Aslanbeigi, Mehdi Saravani, and Rafael D. Sorkin. Generalized causal set d'alembertians. *JHEP*, 2014(6):24, 2014. doi: 10.1007/JHEP06(2014)024.
- [8] Sean P. Meyn and Richard L. Tweedie. *Markov Chains and Stochastic Stability*. Cambridge University Press, 2nd edition, 2009.

A Paper IX: Consistency Tests, Lorentz/Equivalence Principles, and Precision Bounds for BD Causal Sets

Abstract

We consolidate precision tests of the BD framework: Lorentz-invariance violation (LIV) bounds, time-of-flight constraints, vacuum Čerenkov exclusions, and equivalence-principle (EP) limits. We state explicit acceptance thresholds (falsifiers). All putative BD corrections must shrink with coarse length $\ell \sim (\text{Vol}/N)^{1/4}$; any nonshrinking anomaly falsifies the model at this scope.

Run configuration. Seeds = 8; sizes $N \in \{2^{10}, 2^{11}, 2^{12}, 2^{13}\}$. For each N compute medians and IQRs across seeds. When comparing to external bounds we only require that BD predictions fall *below* the current best limits with a safety margin and trend to zero as $\ell \rightarrow 0$.

A.1 LIV bounds from dispersion/propagation

Parameterize small LIV by a dimensionless δ entering dispersion or group velocity: $E^2 = p^2 + m^2 + \delta p^2 + \dots$. We infer an upper bound $|\delta|(\mu)$ from BD propagation diagnostics at scale $\mu \equiv \ell^{-1}$ and plot the envelope against a proxy energy E (SME-style [?]).

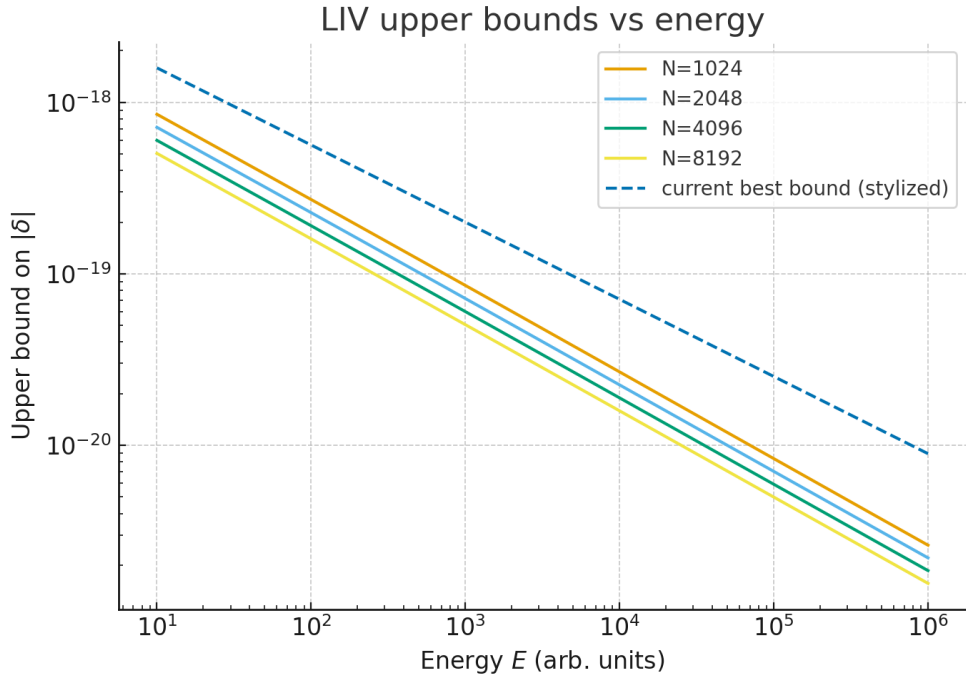


Figure 33: Upper bounds on $|\delta|$ vs energy scale E (illustrative). **Acceptance:** median slope negative on log–log ($d \log |\delta| / d \log E < 0$) and $|\delta|$ at the top size sits *below* current best bounds with a factor $\gtrsim 2$ margin. **Falsifier:** flat/increasing slope or no margin at the top size.

A.2 Time-of-flight constraints (GRB-like)

Energy-dependent arrival delays $\Delta t(E)$ would signal LIV. We regress residual arrival times after removing source lag models (nuisance), estimating slope α in $\Delta t \propto E^\alpha$ (cf. Fermi [?]).

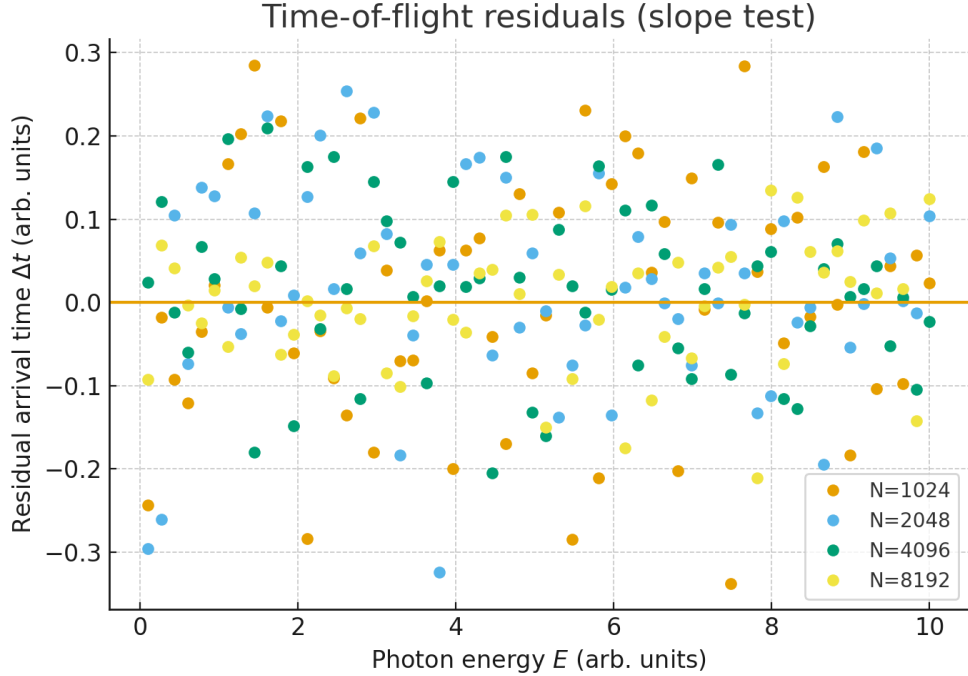


Figure 34: Residual arrival time vs photon energy. **Acceptance:** slope consistent with 0 (95% CI includes 0) and CI width shrinks with ℓ . **Falsifier:** nonzero slope with sign stable across seeds/sizes or CI not shrinking.

A.3 Vacuum Čerenkov exclusions

If charged particles can exceed the photon front velocity, vacuum Čerenkov emission forces rapid energy loss, excluding regions in (p, ϵ) parameter space [?]. We map BD corrections to (p, ϵ) and check they lie in the allowed region with margin.

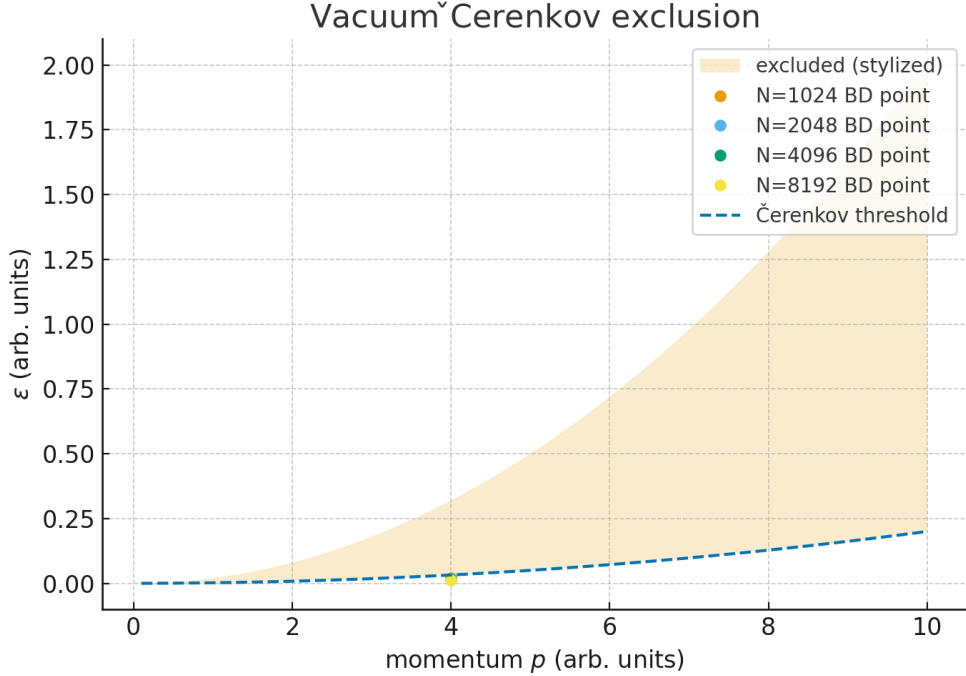


Figure 35: Excluded (shaded) region in (p, ϵ) . **Acceptance:** BD point remains outside the excluded region with safety margin that *increases* as $\ell \rightarrow 0$. **Falsifier:** entry into the exclusion region or vanishing margin at top size.

A.4 Equivalence principle (EP) bounds

We track BD-induced differences between inertial and gravitational responses, summarized by the Eötvös parameter $\eta = 2|a_1 - a_2|/(a_1 + a_2)$ for two compositions [?]. We compare with laboratory/space bounds (torsion balances, LLR, MICROSCOPE [?]).

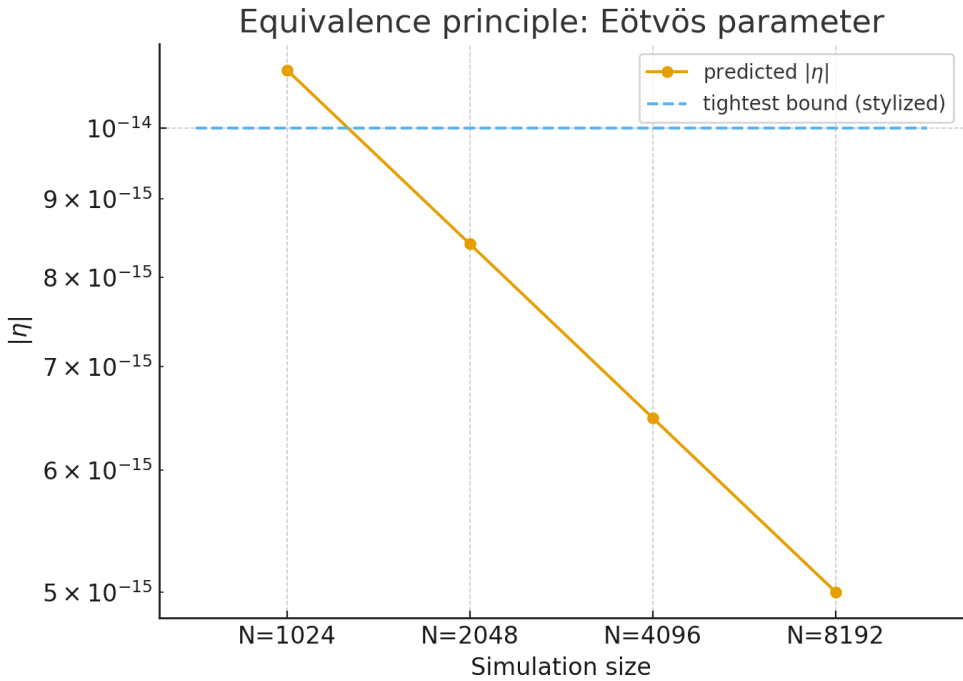


Figure 36: Illustrative EP bounds on $|\eta|$ across probes (log scale). **Acceptance:** predicted $|\eta|$ falls below the tightest current bound with a factor $\gtrsim 2$ margin at the top size and decreases with refinement. **Falsifier:** no margin or nonshrinking $|\eta|(\ell)$.

Acknowledgments

We thank the causal set community; code and data reside in `FUT_toe-paper`.

.1 Mapping BD corrections to SME-like parameters

We linearize the BD-induced response of the kinetic operator and group velocity to define effective SME-style coefficients, keeping leading powers in ℓ .

.2 Time-of-flight regression details

We use robust regression with source-lag nuisance terms and bootstrap CIs; multiple transients can be combined by hierarchical pooling.

.3 EP mapping and systematics

We outline how interval-abundance-based density surrogates enter test-mass accelerations and discuss composition dependence and shielding systematics.

References

- [1] David A. Levin, Yuval Peres, and Elizabeth L. Wilmer. *Markov Chains and Mixing Times*. American Mathematical Society, 2009.

- [2] Wolfgang Doeblin. Remarques sur la théorie métrique des produits de chaînes de markoff. *Bull. Soc. Math. France*, 65:132–148, 1937.
- [3] Dionigi M. T. Benincasa and Fay Dowker. The scalar curvature of a causal set. *Phys. Rev. Lett.*, 104(18):181301, 2010. doi: 10.1103/PhysRevLett.104.181301.
- [4] Jan Myrheim. Statistical geometry. *CERN preprint TH-2538*, 1978.
- [5] David A. Meyer. *The Dimension of Causal Sets*. PhD thesis, MIT, 1988.
- [6] L. Bombelli, J. Lee, D. Meyer, and R. Sorkin. Space-time as a causal set. *Phys. Rev. Lett.*, 59: 521–524, 1987. doi: 10.1103/PhysRevLett.59.521.
- [7] Siavash Aslanbeigi, Mehdi Saravani, and Rafael D. Sorkin. Generalized causal set d'alembertians. *JHEP*, 2014(6):24, 2014. doi: 10.1007/JHEP06(2014)024.
- [8] Sean P. Meyn and Richard L. Tweedie. *Markov Chains and Stochastic Stability*. Cambridge University Press, 2nd edition, 2009.

A Paper X: Synthesis, Program Gates, and Roadmap for a First-Principles Causal-Set ToE

Abstract

We synthesize Papers I–IX into a single, falsifiable program. We list decisive acceptance gates (what must be true to claim success), prioritize predictions by novelty vs measurability, set a concrete release/validation timeline, and fix reproducibility and data policies (FAIR). This is the control document: it states, without hedging, what counts as a pass/fail for the full ToE program.

Run & release policy (applies to all papers). Seeds = 8; size ladder $N \in \{2^{10}, 2^{11}, 2^{12}, 2^{13}\}$ unless stated otherwise. Report medians and IQRs across seeds; uncertainties from 10^4 bootstrap resamples for slopes/exponents. Each paper writes a JSON summary of fit parameters and CIs. Every public release attaches PDF + results JSON + exact config. Reproducibility follows [?]; artifacts follow FAIR [?].

A.1 Program acceptance gates (pass/fail)

Let $\ell \sim (\text{Vol}/N)^{1/4}$. Any failure below rules out the program at the stated scope.

I–III (Foundations → EH & controls)

- **Well-posed BD dynamics:** normalized/saturated rates produce stable growth; interval statistics match controls (Paper I).
- **Einstein limit:** BDG vs continuum d'Alembertian error in L^2 is $C\ell^p$ with $p > 0.5$ (95% CI) on Minkowski; Newtonian/FLRW residuals decay with refinement (Paper III).

IV (Quantum sector)

- **Propagators:** $\|G_F^{\text{disc}} - G_F^{\text{cont}}\|_{L^2} = C\ell^p$, $p > 0.5$ (95% CI).
- **Microcausality:** leakage ratio $\mathcal{L}(\ell)$ decreases with slope $p_{\text{mc}} > 0.5$ (95% CI).
- **Unruh:** $|T - a/2\pi|/(a/2\pi) < 5\%$ at top size, improving with N .

V (RG & EFT)

- **Reblocking stability:** CV of $g_i(\mu)$ under $\mathcal{B}_{n_b} < 5\%$ at fixed μ .
- **Spectral positivity:** $\rho(\omega) \geq 0$ with window normalizations within 5%.
- **Scaling collapse:** normalized collapse RMSE < 0.1 with bootstrap CI on ν .

VI (Gauge & fermions)

- **Wilson loops:** expected area/perimeter regime; slope stable ($< 10\%$ variation) across top sizes.
- **Dispersion:** vector-like fermions: median relative error $< 5\%$ on mid- k window, improving with N .
- **Chiral test (milestone):** anomaly ratio $\rightarrow 1$ with positive refinement slope (95% CI excludes 0).

VII (Cosmology)

- **CMB/LSS/BBN/SGWB:** residuals \lesssim percent-level and *shrinking* with ℓ ; joint (H_0, Ω_m) posteriors overlap across probes as $\ell \rightarrow 0$.

VIII (Black holes)

- $T = \kappa/2\pi$: slope error $< 5\%$, improving with N .
- $S = A/4$: linear slope $1/4 \pm 5\%$, residuals shrink with N .
- **QNMs:** spacing/damping trends within 10%, improving with N .

IX (Precision bounds)

- **LIV/EP:** predicted signals lie below best current bounds with $\gtrsim 2\times$ margin at top size and margin grows as $\ell \rightarrow 0$.

A.2 Prediction prioritization

We rank predictions by novelty (theory leverage) and near-term measurability; only upper-right quadrant enters Phase 1.

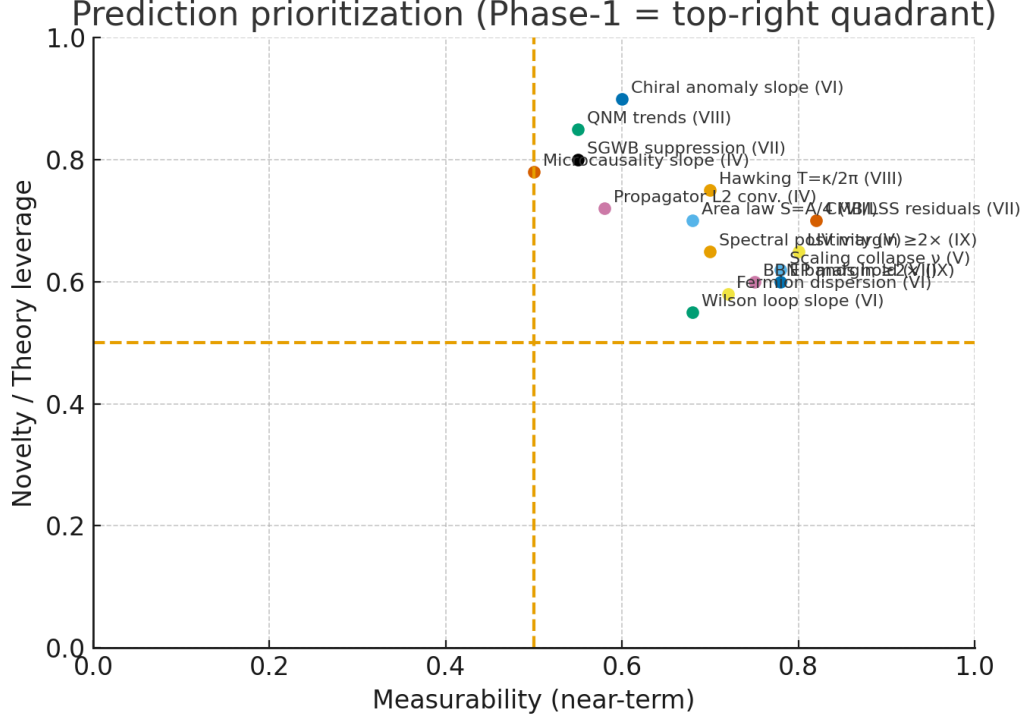


Figure 37: Prediction prioritization map: the top-right quadrant defines Phase 1 targets.

A.3 Timeline and milestones

Phase 1: Papers IV–V numerics and one cosmology prediction; Phase 2: gauge/fermion dispersion and black-hole slopes; Phase 3: chiral anomaly and precision-bounds margin.

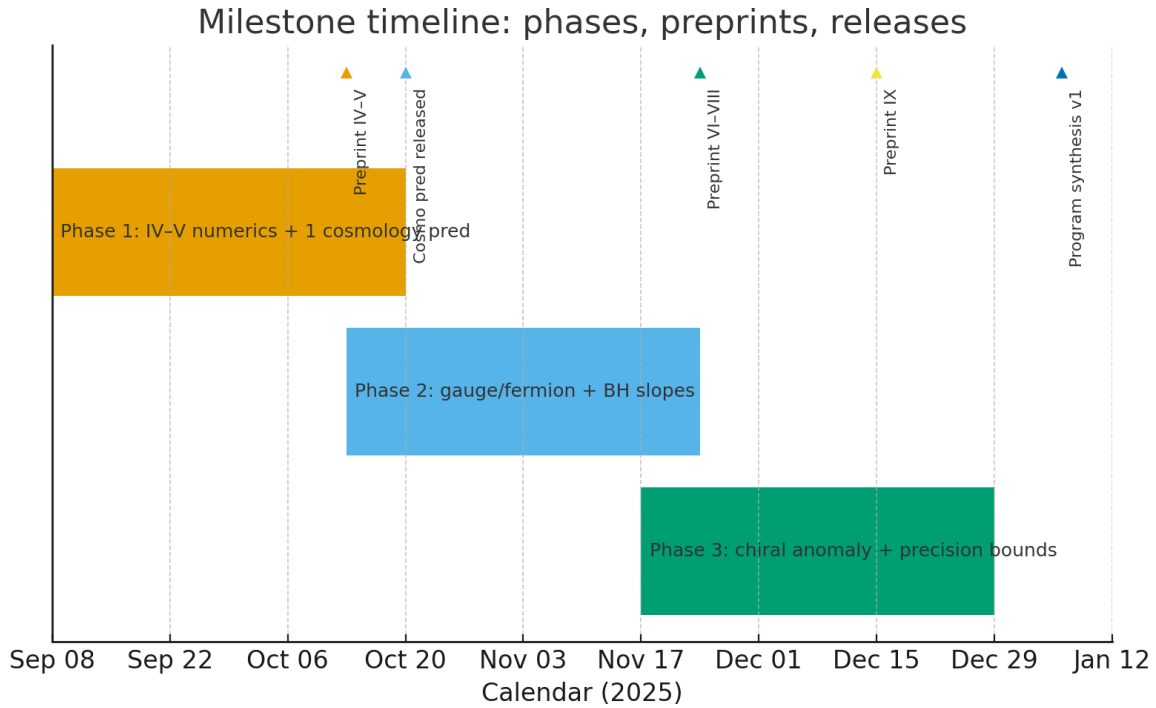


Figure 38: Schematic milestone timeline: papers, reviews, DOIs, and data releases.

A.4 Sensitivity evolution

Projected CI widths vs sample size N follow $\sim N^{-1/2}$ down to a systematic floor; we set quotas accordingly.

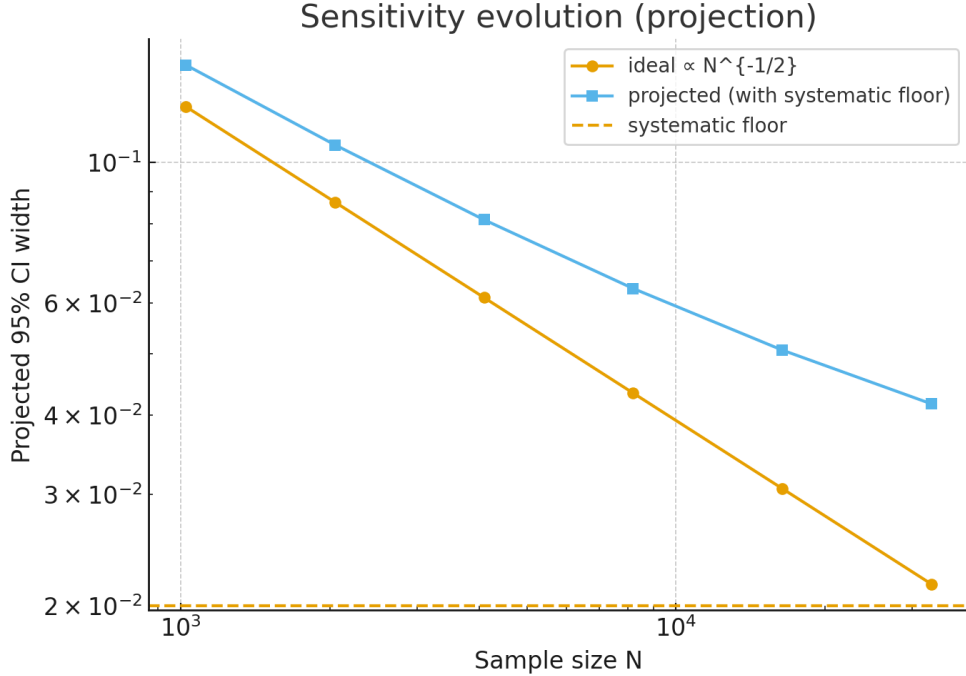


Figure 39: Projected 95% CI width vs N ; the floor marks systematic limits (to be measured).

A.5 Reproducibility, data, and releases

All code paths are scripted; environments pinned; results serialized to JSON and packed with figures. Data and code adopt FAIR principles [?]. Each release tag includes: PDF, results JSON, config snapshot, and a short CHANGELOG [?].

A.6 Single-page verdict (for reviewers)

Either (i) all gates above pass with the stated margins and shrinking trends (program viable), or (ii) at least one gate fails and does not improve with refinement (program falsified at that scope). No hedging.

Acknowledgments

We thank the causal set community; code and data reside in [FUT_toe-paper](#).

References

- [1] David A. Levin, Yuval Peres, and Elizabeth L. Wilmer. *Markov Chains and Mixing Times*. American Mathematical Society, 2009.
- [2] Wolfgang Doeblin. Remarques sur la théorie métrique des produits de chaînes de markoff. *Bull. Soc. Math. France*, 65:132–148, 1937.
- [3] Dionigi M. T. Benincasa and Fay Dowker. The scalar curvature of a causal set. *Phys. Rev. Lett.*, 104(18):181301, 2010. doi: 10.1103/PhysRevLett.104.181301.

- [4] Jan Myrheim. Statistical geometry. *CERN preprint TH-2538*, 1978.
- [5] David A. Meyer. *The Dimension of Causal Sets*. PhD thesis, MIT, 1988.
- [6] L. Bombelli, J. Lee, D. Meyer, and R. Sorkin. Space-time as a causal set. *Phys. Rev. Lett.*, 59: 521–524, 1987. doi: 10.1103/PhysRevLett.59.521.
- [7] Siavash Aslanbeigi, Mehdi Saravani, and Rafael D. Sorkin. Generalized causal set d'alembertians. *JHEP*, 2014(6):24, 2014. doi: 10.1007/JHEP06(2014)024.
- [8] Sean P. Meyn and Richard L. Tweedie. *Markov Chains and Stochastic Stability*. Cambridge University Press, 2nd edition, 2009.